Female-germline specific protein Sakura interacts with Otu and is crucial for germline stem cell renewal and differentiation and oogenesis

Azali Azlan[1], Li Zhu[1], and Ryuya Fukunaga[1*]

[1]*Department of Biological Chemistry, Johns Hopkins School of Medicine, Baltimore, MD 21205*

*Corresponding author

Email: (fukunaga@jhmi.edu)

Abstract

During oogenesis, self-renewal and differentiation of germline stem cells (GSCs) must be tightly regulated. The *Drosophila* female germline serves as an excellent model for studying these regulatory mechanisms. Here, we report that a previously uncharacterized gene *CG14545*, which we named *sakura*, is essential for oogenesis and female fertility in *Drosophila*. Sakura is predominantly expressed in the ovaries, particularly in the germline cells, including GSCs. *sakura* null mutant female flies display rudimentary ovaries with germline-less and tumorous phenotypes, fail to produce eggs, and are completely sterile. The germline-specific depletion of *sakura* impairs Dpp/BMP signaling, leading to aberrant *bag-of-marbles* (*bam*) expression, resulting in faulty differentiation and loss of GSCs. *sakura* is also necessary for normal levels of piwi-interacting RNAs (piRNAs) levels and for female-specific splicing of *sex-lethal* (*sxl*), a master regulator of sex identity determination. We identified Ovarian Tumor (Otu) as a protein binding partner of Sakura and found that loss of *otu* phenocopies loss of *sakura* in ovaries. Thus, we identify Sakura

21 as a crucial factor for GSC renewal and differentiation and oogenesis, and propose that Sakura and

22 Otu function together in these processes.

23

24 **Introduction**

25 Oogenesis is a complex process in which germline stem cells (GSCs) develop into mature female
26 gametes or oocytes. This process involves multiple layers of regulations and numerous genes,
27 some of which remain to be discovered and characterized. *Drosophila melanogaster*, a genetically
28 tractable model organism, has long been at the forefront of GSC and oogenesis research (Kirilly
29 and Xie 2007).

30 Adult *Drosophila* females possess a pair of ovaries, each composed of 12-16 ovarioles. At
31 the anterior tip of each ovariole is a structure called the germarium, which houses two to three
32 GSCs (Fig 1A). GSCs reside in the most anterior region of the germarium, where they directly
33 contact cap cells and escort cells, forming a niche crucial for GSC self-renewal (Lin and Spradling
34 1993; de Cuevas and Matunis 2011; Losick et al. 2011). GSCs undergo asymmetric mitotic
35 division, producing two distinct cells: one GSC and one cystoblast. The cystoblast, destined to
36 differentiate, undergoes four mitotic divisions with incomplete cytokinesis, resulting in
37 interconnected cysts of 2, 4, 8, and 16 cells. Of the 16 cells, one will differentiate into an oocyte,
38 while the remaining 15 develop into polyploid nurse cells, which synthesize proteins and RNAs
39 for deposition into the oocyte.

40 GSCs must be tightly regulated to maintain their undifferentiated state while dividing and
41 differentiating to produce one GSC and one cystoblast. Failure in GSC self-renewal or
42 inappropriate differentiation leads to stem cell loss, disrupting oocyte production (Lin 1997; Cox
43 et al. 1998). Conversely, uncontrolled GSC division or defective differentiation results in an
44 overabundance of GSC-like cells (a tumorous phenotype) and fewer differentiated cells,
45 ultimately inhibiting oocyte production (Gateff et al. 1996; Ohlstein et al. 2000). Thus, a precise

46 balance between GSC self-renewal and cyst differentiation within the germarium is essential for
47 proper oogenesis and is tightly regulated.

48 Bone Morphogenetic Protein (BMP) signaling plays a critical role in regulating GSC self-
49 renewal and differentiation during *Drosophila* oogenesis. In the stem cell niche, GSCs are
50 physically anchored to cap cells via adherens and gap junctions (Song et al. 2002; Gilboa et al.
51 2003). Cap cells secrete BMP ligands, such as Decapentaplegic (Dpp) and Glass bottom boat
52 (Gbb), which are recognized by transducing receptors like Thickvein (Tkv) and Saxophone (Sax)
53 on the GSCs (Fig S1) (Xie and Spradling 1998; Casanueva and Ferguson 2004). Upon activation,
54 these receptors phosphorylate a transcription factor Mad. The phosphorylated Mad (pMad)
55 translocates into the nucleus, where it represses the transcription of *bag-of-marbles* (*bam*), a key
56 differentiation factor (Kai and Spradling 2003; Song et al. 2004).

57 Bam, a ubiquitin-associated protein, is essential for cystoblast differentiation (McKearin
58 and Spradling 1990; McKearin and Ohlstein 1995). Dpp/BMP signaling in the niche represses *bam*
59 expression, preventing GSCs from differentiating and enabling self-renew (Song et al. 2004).
60 However, as the daughter cells (cytoblasts) exit the niche, they derepress *bam* and initiate the
61 differentiation program (Fig S1). Tight regulation of Dpp/BMP signaling and *bam* expression
62 ensures that only cells within the niche adopt GSC fate, while adjacent daughter cells differentiate
63 into cystoblasts. Loss of *bam* leads to blocked differentiation and the accumulation of GSC-like
64 cells (tumorous phenotype), whereas ectopic *bam* expression forces GSCs differentiation,
65 depleting the stem cell pool (McKearin and Spradling 1990; McKearin and Ohlstein 1995;
66 Ohlstein and McKearin 1997).

67 One of the proteins that interacts with Bam is Ovarian Tumor (Otu) (Ji et al. 2017). Otu
68 forms a deubiquitinase complex with Bam, which deubiquitinates Cyclin A (CycA), stabilizing

69 CycA and promoting GSC differentiation (Ji et al. 2017). Otu also binds RNAs (Ji et al. 2019).
70 Otu is crucial for oogenesis and female fertility. Mutations in the *otu* gene cause various ovarian
71 defects, including tumorous growths, germ cell loss, abnormalities in oocyte determination and
72 nurse cell dumping, and defects in the sexual identity determination of germ cells, indicating Otu's
73 importance in multiple stages of oogenesis (Smith and King 1966; Gans et al. 1975; Gollin and
74 King 1981; King and Riley 1982; Storto and King 1988; Pauli et al. 1993; Rodesch et al. 1997;
75 Glenn and Searles 2001). However, the precise molecular mechanisms by which Otu functions in
76 these processes remain largely unknown.

77 In this study, we aimed to identify a novel gene required for oogenesis. Through a search
78 for uncharacterized genes expressed exclusively in *Drosophila* ovaries, we discovered *CG14545*,
79 a gene encoding a 114 amino acids (aa) long protein without any known functional domain (Fig
80 1B). We found that CG14545 is expressed specifically in female germline cells, including GSCs.
81 Our genetic analysis revealed that *CG14545* is required for oogenesis and female fertility and plays
82 an important intrinsic role in regulating GSCs renewal and differentiation. Additionally, CG14545
83 is important for the piRNA pathway and for the female-specific mRNA splicing pattern of *sex-*
84 *lethal* (*sxl*), a master regulator of sex determination. We identified Otu as a binding partner of the
85 CG14545 protein, suggesting that both proteins may participate in the same molecular pathways
86 to regulate GSC fate and differentiation. We named the *CG14545* gene *sakura*, meaning "cherry
87 blossom" in Japanese, symbolizing birth and renewal.

88

89 **Results**

90 **Sakura is exclusively expressed in the ovaries**

Based on high-throughput expression data in Flybase, *sakura* mRNA is highly and exclusively expressed in adult ovaries (Fig S2). To investigate Sakura protein expression, we generated a polyclonal anti-Sakura antibody against a recombinant full-length Sakura protein. Using this antibody, we examine Sakura protein expression at different stages of *Drosophila* development and across tissues. We found that Sakura protein is specifically expressed in ovaries, particularly in stage 1-11 egg chambers (Fig 1C).

sakura mutant flies

To explore the biological and molecular functions of Sakura *in vivo*, we generated a *sakura* mutant allele ($sakura^{null}$) with a one nucleotide (nt) insertion replacing 33 nts within the Sakura coding region using the CRISPR/Cas9 genome editing system (Fig 1B). This mutation causes a frameshift and a premature stop codon, resulting in a 33-amino acid (aa) N-terminal fragment of Sakura followed by a 22-aa segment produced by frameshifted translation (Fig 1B). This truncated fragment is unlikely to be functional, and we were unable to detect stable protein expression, as shown below (Fig 1D). Thus, we consider this allele a null mutation. $sakura^{null/null}$ flies were viable, revealing that Sakura is not essential for survival.

To validate the $sakura^{null}$ strain, we performed Western blots using ovary lysates from *sakura* mutant flies using the anti-Sakura antibody. As expected, full-length Sakura protein was detected in the ovaries of wild-type ($sakura^{+/+}$) and heterozygous controls ($sakura^{null/+}$), but not in those of homozygous mutants ($sakura^{null/null}$) (Fig 1D). No smaller protein corresponding to the

112 truncated Sakura fragment was detected in either *sakura*$^{null/+}$ or *sakura*$^{null/null}$ ovaries thus,
113 suggesting that the fragment is unstable or not expressed.

114

115 **Sakura is cytoplasmic and expressed specifically in germ cells**

116 To determine the localization of Sakura protein within the ovaries, we generated transgenic flies
117 carrying a Sakura coding sequence fused with EGFP at the C-terminus (Sakura-EGFP) under the
118 control of the *sakura* promoter. Western blot analysis of ovary lysates showed that Sakura-EGFP
119 is expressed at levels comparable to endogenous Sakura (Fig 1D).

120 Oogenesis begins in the germarium, which contains 2-3 GSCs identified by round,
121 unbranched spectrosomes that contact cap cells (Fig 1A) (Kirilly and Xie 2007). In contrast, cysts
122 exhibit branched fusomes. Immunostaining with hu-li tai shao (HTS) antibody marks both
123 spectrosomes and fusomes (Fig 1E), while Vasa is a known germ cell marker (Fig 1F). Confocal
124 imaging revealed that Sakura-EGFP is specifically expressed in the cytoplasm of germ cells,
125 including GSCs, cyst cells, nurse cells, and developing oocytes (Fig 1E and 1F). Sakura-EGFP
126 was not expressed in somatic cells such as terminal filament, cap cells, escort cells, or follicle cells.
127 (Fig 1E). In the egg chamber, Sakura-EGFP was detected in the cytoplasm of nurse cells and was
128 enriched in developing oocytes (Fig 1F).

129

130 ***sakura* is essential for female fertility**

131 Given its ovary-specific expression at both mRNA and protein levels (Fig 1C and S2), we
132 hypothesized that Sakura plays a critical role in ovarian function. Fertility assays revealed that

133 *sakura*$^{null/null}$ females laid no eggs when mated with wild-type males, while control females
134 (*sakura*$^{+/+}$ and *sakura*$^{null/+}$) laid numerous eggs (Fig 2A and 2B). Dissection of *sakura*$^{null/null}$ ovaries
135 revealed that they were rudimentary compared to normal ovaries in controls (Fig 2C). This
136 suggests that the inability of *sakura*$^{null/null}$ female to lay eggs is due to their underdeveloped ovaries.
137 In contrast, *sakura*$^{null/null}$ males were fertile and showed no significant differences compared to
138 controls (*sakura*$^{+/+}$ and *sakura*$^{null/+}$) (Fig S3).

139 To confirm that the observed female sterility was caused by the loss of *sakura*, we
140 generated *sakura* rescue flies expressing Sakura-EGFP in the *sakura*$^{null/null}$ background
141 (*sakura*$^{null/null}$; *sakura-EGFP*). Western blotting confirmed that these flies expressed Sakura-EGFP,
142 but not endogenous Sakura (Fig 1D). The *sakura-EGFP* transgene fully rescued both female
143 fertility and ovary morphology in the *sakura*$^{null/null}$ background (Fig 2). *sakura-EGFP* rescue
144 females showed no significant fertility differences compared to controls (Fig 2A and 2B), and their
145 ovaries were normal in shape and size (Fig 2C). We concluded that Sakura is essential for female
146 fertility and normal ovary morphology but dispensable for male fertility, consistent with the
147 observation that Sakura is predominantly expressed in ovarian germline cells (Fig 1).

148

149 **_sakura_$^{null/null}$ ovaries are germless and tumorous**

150 Given the rudimentary appearance of *sakura*$^{null/null}$ ovaries, we questioned whether they contained
151 germ cells. We used flies carrying *vasa-EGFP* knocked-in reporter in the *sakura*$^{null/null}$ background,
152 as Vasa is a known germ cell marker. We observed that some *sakura*$^{null/null}$ ovarioles were devoid
153 of germ cells ("germless", cyan stars), while others retained germ cells (Fig 3A and 3B).
154 Immunostaining with HTS antibody revealed an excess number of GSC-like cells with round

155 spectrosomes in *sakura*$^{null/null}$ ovarioles containing germ cells (Fig 3C, orange stars), indicative of
156 a "tumorous" phenotype as previously described for mutants of other genes including *bam*, *otu*,
157 and *sxl* (Smith and King 1966; Gans et al. 1975; Gollin and King 1981; King and Riley 1982;
158 McKearin and Spradling 1990; Bopp et al. 1993; Eliazer et al. 2011; Jin et al. 2013; Yang et al.
159 2019). Additionally, we observed an excess number of cyst cells with branched fusomes that
160 persisted throughout the ovarioles, suggesting abnormal cyst cell differentiation and division.
161 Thus, loss of *sakura* results in both germ cell depletion and overgrowth.

162 Within the same ovary, some *sakura*$^{null/null}$ ovarioles exhibited the tumorous phenotype,
163 while others were germless, without any spectrosome or fusome staining (Fig 3A-3C, cyan stars).
164 Quantification revealed that 35% of *sakura*$^{null/null}$ ovarioles from 2- to 5-day-old flies were
165 tumorous, while the remaining 65% were germless (n=74) (Fig 3D). In contrast, all ovarioles in
166 control (*sakura*$^{+/+}$ and *sakura*$^{null/+}$) and *sakura-EGFP* rescue flies were normal with no tumorous
167 or germless phenotypes observed (Fig 3D). Approximately 95% of *sakura*$^{null/null}$ ovarioles
168 containing germ cells had an excess of GSC-like cells (>5) (Fig 3E and Fig S4). The mean number
169 of GSCs or GSC-like cells in 2- to 5-day-old *sakura*$^{+/+}$, *sakura*$^{null/+}$, and *sakura-EGFP* rescue was
170 2.2 ± 0.6, 2.2 ± 0.6, and 2.1 ± 0.7, respectively while that for *sakura*$^{null/null}$ was 26.5 ± 17.5 (p-
171 value <0.05).

172 We investigated the age-dependent effects on the tumorous and germless phenotypes by
173 examining the ovarioles from 0-1 day old, 7-day old, and 14-day old flies. Ovarioles in control and
174 *sakura-EGFP* rescue flies remained normal throughout this time course (Fig S5A). In the very
175 young, 0-1 day old *sakura*$^{null/null}$, 78% of ovarioles were tumorous and 22% were germless.
176 Overtime, the ratio of germless ovarioles increased while the ratio of tumorous ovarioles
177 decreased. By 14 days old, only 5% of ovarioles were tumorous, with the remaining 95% being

178 germless. The number of GSC-like cells in *sakura*$^{null/null}$ ovarioles was already high in 0-1 day old
179 flies, and it decreased over time (Fig S5B). Tumorous ovarioles, but not germless ones, exhibited
180 significantly higher levels of cleaved Caspase-3 staining, indicative of apoptosis, compared to
181 controls (Fig 3F). These results suggest that tumorous ovarioles undergo apoptosis, and that these
182 ovarioles eventually become germless.

183 Together, these results suggest that Sakura is essential for regulating the survival,
184 proliferation, and differentiation of germline cells, including GSCs.

185

186 **Loss of *sakura* results in reduced germline piRNA**

187 In controls, Vasa-EGFP is enriched in the perinuclear structure known as the nuage within nurse
188 cells (Fig 3A and 3B), which is essential for piwi-interacting RNA (piRNA) biogenesis. In
189 *sakura*$^{null/null}$ tumorous ovarioles, Vasa-EGFP retains its perinuclear localization, indicating that
190 *sakura* is not required for the proper localization of Vasa to the nuage.

191 piRNAs are produced in germline cells and somatic follicle cells and transcriptionally and
192 post-transcriptionally silence transposon expression through sequence-complementarity (Huang et
193 al. 2017; Yamashiro and Siomi 2018). Disruption of the piRNA pathway can result in oogenesis
194 arrest, germ cell loss, rudimentary ovaries, and sterility. Loss of piRNAs in germ cells leads to the
195 upregulation (desilencing) of transposons, increased DNA damage, and apoptotic cell death[31]. We
196 investigated whether the loss of *sakura* would result in loss of piRNA and transposon upregulation.
197 We performed high-throughput sequencing (small RNA-seq and polyA+ RNA-seq) on ovary RNA
198 samples from *sakura*$^{+/+}$, *sakura*$^{null/+}$, *sakura*$^{null/null}$, and *sakura-EGFP* rescue (*sakura*$^{null/null}$ with
199 *sakura-EGFP*) flies.

200 piRNA levels in *sakura*$^{null/null}$ ovaries were reduced compared to controls (*sakura*$^{+/+}$), while
201 *sakura*$^{null/+}$ and *sakura-EGFP* rescue showed no such reduction (Fig 4A). Consistent with this,
202 transposon RNA levels in *sakura*$^{null/null}$ ovaries were upregulated compared to *sakura*$^{+/+}$, while
203 *sakura*$^{null/+}$ and *sakura-EGFP* rescue showed no such upregulation (Fig 4B). Given that Sakura is
204 specifically expressed in germline cells, but not in somatic cells (Fig 1E and 1F), we hypothesized
205 that loss of *sakura* interrupts the piRNA pathway in germ cells, leading to the desilencing of
206 germline transposons. A well-characterized germline transposon in *Drosophila* is *Burdock*
207 (Donertas et al. 2013; Handler et al. 2013). We found that *Burdock* piRNA levels were significantly
208 lower in *sakura*$^{null/null}$ compared to controls and rescue flies (Fig 4C).

209 We employed the *Burdock* sensor, a transposon reporter tool to monitor germline piRNA
210 activity (Handler et al. 2013). The reporter expresses nuclear GFP and β-gal under the control of
211 the *nanos* promoter for germline expression, with a target sequence for *Burdock* piRNAs in the 3′
212 UTR (Fig 4D). Using a *sakura* RNAi line driven by *UAS-Dcr2* and *NGT-Gal4* to knock down
213 *sakura* specifically in the germline, we observed that GFP and β-gal expression were highly
214 elevated in *sakura* knockdown germlines compared to control RNAi (y^{RNAi}) knockdowns (Fig 4D).
215 This confirmed that loss of *sakura* leads to a loss of piRNA-mediated transposon silencing in the
216 germline, suggesting that Sakura is essential for proper piRNA levels and piRNA-based transposon
217 silencing in the germline.

218

219 **Sex-specific *sxl* mRNA alternative splicing is dysregulated in *sakura*$^{null/null}$ ovaries**

220 Sxl is a master regulator of sex determination in *Drosophila* (Penalva and Sanchez 2003; Salz and
221 Erickson 2010; Grmai et al. 2022). Sex-specific alternative splicing of *sxl* transcripts produces

222 distinct mRNA isoforms: the female-specific and male-specific mRNA isoforms in respective sex
223 and only the female-specific mRNA isoform encodes the functional Sxl protein, whereas the male-
224 specific isoform does not. In the female germline, loss of Sxl function or disruption of female-
225 specific *sxl* splicing leads to developmental defects, including germline tumors and sterility.
226 Notably, several mutants with tumorous ovariole phenotypes—including *otu* mutants—exhibit
227 aberrant *sxl* mRNA splicing, resulting in the expression of the male-specific isoform in ovaries and
228 defects in germ cell sexual identity (Bopp et al. 1993; Pauli et al. 1993).

229 We examined *sxl* splicing in *sakura* mutants. As expected, ovaries from control and *sakura-*
230 *EGFP* rescue flies expressed exclusively the female-specific *sxl* mRNA isoform and testes from
231 control flies expressed only the male-specific isoform (Fig S6). In contrast, *sakura*$^{null/null}$ ovaries
232 exhibited the male-specific isoform and a reduced level of the female-specific isoform. These
233 results indicate that female-specific *sxl* alternative splicing is disrupted in the absence of *sakura*.

234

235 ***sakura* is important for oogenesis in germline cells beyond GSCs and germline cysts**

236 Both *sakura*$^{null/null}$ and *sakura* germline RNAi knockdown driven by *UAS-Dcr-2* and *NGT-Gal4*,
237 which initiates RNAi in germline from GSCs, resulted in rudimentary ovaries (Fig 2C and 5A).
238 These ovaries lacked later-stage germline cells and egg chambers, making it difficult to assess the
239 role of Sakura beyond the germarium. However, because Sakura-EGFP expression is not limited
240 to GSCs and germline cysts (Fig 1E and 1F), we speculated that Sakura might function in later-
241 stage germline cells as well.

242 To explore this possibility, we used *TOsk-Gal4* (a combination of *osk-Gal4* and *αTub67C-*
243 *Gal4*) to drive *sakura* RNAi knockdown in germline cells after the germline cyst stage (from

germarium region 2b onward. Fig 1A), sparing GSCs and germline cysts (ElMaghraby et al. 2022). Unlike *NGT-Gal4*, *TOsk-Gal4*-driven *sakura* RNAi knockdown did not drastically affect ovary morphology (Fig 5A), allowing us to study the effects of *sakura* loss in egg chambers. We confirmed *sakura* RNAi (*sakura RNAi #1* and #2) knockdown efficiency by Western blot, showing effective depletion of Sakura in ovaries from both *NGT-Gal4* and *TOsk-Gal4*-driven RNAi lines (Fig 5B).

Interestingly, *TOsk-Gal4*-driven *sakura* RNAi knockdown severely reduced the numbers of eggs laid (Fig 5C) and stage 14 oocytes in ovaries compared to control RNAi (y^{RNAi}) (Fig 5D), suggesting that *sakura* is important for oogenesis beyond the germline cyst stage. Additionally, we observed mislocalized and dispersed Oo18 RNA-binding protein (Orb), a marker for oocyte identity, in *TOsk-Gal4*-driven *sakura* RNAi ovaries beginning around stage 6 of oogenesis (Fig

5E). In controls, Orb was enriched and properly localized to the posterior end of stage ~6-8 egg chambers (Fig 5E, yellow arrows). In $sakura^{RNAi}$ ovaries, although Orb localization appeared normal at stage ~6 (yellow arrow), mislocalization was evident by stage ~8 (magenta arrow), and signs of cytoskeletal disorganization were apparent in later-stage egg chambers (white arrowheads). Phalloidin staining to visualize F-actin further supported cytoskeletal defects in $sakura^{RNAi}$ later-stage egg chambers (Fig S7).

These defects likely contribute to the impaired production of stage 14 oocytes and eggs in $sakura^{RNAi}$ flies (Fig 5C and 5D). We conclude that Sakura plays an essential role in oogenesis beyond the early germline stages. For all subsequent *sakura* RNAi experiments, we used the *sakura RNAi* #2 line.

266 **Sakura is required intrinsically for GSC establishment, maintenance, and differentiation**

267 To investigate whether *sakura* functions autonomously in the germline, we performed mosaic
268 analysis using the FLP-FRT system with heat shock promoter-driven FLP (*hs-flp*) (Xu and Rubin
269 1993; Rubin and Huynh 2015). First, to assesse its role in GSC establishment, we induced
270 *sakura*^{null} clones in primordial germ cells (PGCs) by applying heat shock before the early third
271 instar larval stage and tracked their development into adult GSCs, following a previously
272 established protocol (Yang et al. 2007). In control adult flies (*FRT82B*),12.3% (20/163) of GSCs
273 were marked, wheras only 1.9% (4/213) were marked in *sakura*^{null} mutants (*FRT82B*, *sakura*^{null})
274 (p-value = $4.8 * 10^{-11}$, chi-square test), indicating that *sakura* is autonomously required for GSC
275 establishment.

276 Next, we assessed GSC maintenance using the same system by generating *sakura*^{null} GSC
277 clones in adult flies and measuring clone loss over time, as described previously (Xie and Spradling
278 1998; Yang et al. 2007). Four days after clone induction, 27.8% of GSCs were marked in controls
279 (*FRT82B*) and 22.1% in *sakura*^{null} (*FRT82B*, *sakura*^{null}), which we defined as initial levels (Fig
280 6A). In controls, the percentage of marked GSCs declined to 25.8% on day 7 and and 16.8% on
281 14, resulting in a 39.4% loss rate over 10 days (from day 4 to day 14). In contrast, the proportion
282 of marked *sakura*^{null} GSC clones dropped more sharply—to 16.3% on day 7 and and 5.4% on day
283 14—yielding a higher loss rate of 75.6% over 10 days. These results demonstrate that *sakura* is
284 intrinsically important for GSC maintenance.

285 We further tested whether *sakura* is intrinsically required for GSC differentiation, we
286 quantified the number of marked (GFP-negative) and unmarked (GFP-positive) GSC-like cells
287 (germline cells with a round spectrosome) in the germaria containing marked GSC clones at days
288 4, 7, and 14 post-induction (Fig 6B). We found that marked *sakura*^{null} GSC-like cells were

289 significantly more numerous than marked control GSC-like cells at all time points (Fig 6C). The
290 number of marked *sakura*^{null} GSC-like cells increased over the 10-day period, while the number
291 of marked control cells did not (Fig 6C). In contrast, unmarked GSC-like cells in germaria
292 containing *sakura*^{null} GSC clones did not differ significantly in number compared with those in
293 germaria containing marked control GSC clones, and the number did not increase over time (Fig
294 S8).

295 These results demonstrate that *sakura* is intrinsically important in germline cells, including
296 GSCs, to regulate proper division and differentiation. In the absence of intrinsic *sakura*, germline
297 cells become tumorous and undergo uncontrolled proliferation. Taken together, we conclude that
298 *sakura* is required intrinsically for GSC establishment, maintenance, and differentiation.

299

300 **Loss of *sakura* inhibits Dpp/BMP signaling**

301 The Dpp/BMP signaling pathway plays a central role in regulating *bam* expression and GSC self-
302 renewal and differentiation (Fig S1) (Kirilly and Xie 2007; Hayashi et al. 2020). We
303 hypothesized that the germless and tumorous phenotypes observed in *sakura* loss-of-function
304 ovaries could be due to Dpp/BMP signaling misregulation. To test this, we knocked down *sakura*
305 in the germline driven by *UAS-Dcr2* and *NGT-Gal4* in the presence of *bam-GFP* reporter (Chen
306 and McKearin 2003b). In controls (y^{RNAi}), Bam-GFP expression was restricted to 8-cell cysts and
307 disappeared in 16-cell cysts and onward (Fig 7A). In contrast, *sakura* knockdowns ovaries showed
308 persistent Bam-GFP expression throughout the germarium including the GSC niche region (Fig
309 7A).

310 To further confirm this finding, we used the FLP-FRT system to induce *sakura*^{null} clones in
311 germaria and performed immunostaining with anti-Bam antibody. In control clones (*FRT82B*),
312 Bam expression was observed exclusively in 8-cell cysts. However, in all *sakura*^{null} clones
313 (*FRT82B*, *sakura*^{null}), Bam was aberrantly expressed throughout the germarium, including in GSCs
314 (Fig 7B). These results suggest that in the absence of *sakura*, Bam expression is no longer
315 repressed by Dpp/BMP signaling in the GSC niche, leading to GSC loss, and is no longer shut off
316 after the 16-cell cyst stage.

317 In GSCs, pMad translocates into the nucleus to repress Bam expression (Fig S1) (Kai and
318 Spradling 2003; Song et al. 2004). We stained ovaries with anti-pMad antibodies and found that
319 pMad intensity was significantly reduced in *sakura*^{null} GSC clones compared to control GSCs (Fig
320 7C and D). This indicates that the dysregulated Bam expression observed in *sakura*^{null} was due to
321 reduced pMad levels in GSCs.

322 Previous studies have shown that ectopic expression of a stable form of CycA leads to germ
323 cell loss (Chen et al. 2009). This germ cell loss phenotype is also observed upon ectopic *bam*
324 expression in GSCs (Xie and Spradling 1998; Chen and McKearin 2003a; Xia et al. 2010). It was
325 reported that Bam associates with Ovarian tumor (Otu) to promote deubiquitination and
326 stabilization of CycA (Ji et al. 2017). Since we observed derepressed *bam* expression in *sakura*^{null}
327 cells, we investigated whether CycA levels were affected. Staining ovaries with anti-CycA
328 antibodies revealed higher CycA intensity in *sakura*^{null} clones compared to neighboring wild-type
329 cells in the same germarium (*FRT82B*, *sakura*^{null}) and control clones in control germarium
330 (*FRT82B*) (Fig 7E). *sakura*^{null} clones exhibited significantly higher mean CycA intensity compared
331 to control clones (Fig 7F). The elevated CycA levels in *sakura*^{null} clones likely results from Bam
332 misexpression and Bam-mediated stabilization.

333 To determine whether *bam* misexpression occurs in egg chambers in *sakura* knockdown
334 conditions, we examined *bam* expression in TOsk-Gal4-driven *sakura* RNAi flies. Bam was
335 appropriately restricted to 8-cell cysts in germaria and not misexpressed in egg chambers
336 compared to yRNAi controls (Fig. S9, cyan arrowheads). Thus, *sakura* is specifically required in
337 GSCs and cyst cells to regulate *bam* expression.

338 We also examined DE-Cadherin (DE-Cad), which plays a role in oocyte positioning
339 within the egg chamber (Godt and Tepass 1998). DE-Cad level and localization appeared normal
340 in both control and *sakura* RNAi ovaries through approximately stage 8. However, later-stage
341 egg chambers in *sakura* RNAi flies displayed structural disorganization (Fig. S9, white
342 arrowheads), consistent with defects observed in Fig. 5E and Fig. S7.

343

344 **Attempts to rescue *sakura* loss-of-function ovariole phenotypes**

345 To determine whether the phenotypes caused by *sakura* loss-of-function could be rescued, we first
346 performed genetic interaction experiments by knocking down either *bam* or *cycA* in the germline.
347 As expected, germline-specific *bam* RNAi driven by *UAS-Dcr2* and *NGT-Gal4* resulted in 100%
348 tumorous ovarioles, while *cycA* RNAi produced 100% normal ovarioles in 2–5-day-old flies (Fig.
349 S10A). Double knockdown of *sakura* and *bam* reduced the proportion of germless ovarioles and
350 increased the proportion of tumorous ovarioles compared to *sakura* RNAi alone or the double
351 knockdown of *sakura* and control *w* RNAi. However, no normal ovarioles were observed (Fig.
352 S10A). *sakura* and *cycA* double knockdown had no effect on the phenotype distribution,
353 suggesting that the germless phenotype in *sakura* mutants is partially attributable to ectopic *bam*
354 expression but not to *cycA* misregulation.

The number of GSC-like cells was increased in *sakura* and *bam* double knockdowns compared to *sakura* RNAi or *sakura* and *w* double RNAi, whereas *sakura* and *cycA* knockdown did not alter GSC-like cell numbers (Fig. S10B), , further supporting a genetic interaction between *sakura* and *bam*.

Next, we tested whether the *sakura* loss-of-function phenotypes could be rescued by overexpressing components of the Dpp/BMP signaling pathway. Germline expression of *UASp-Mad-GFP* driven by *nos-Gal4-VP16* in both $sakura^{null/+}$ controls and $sakura^{null/null}$ did not alter the proportions of ovariole phenotypes (Fig S11A) or the number of GSC-like cells (Fig S11B). Thus, transgenic overexpression of Mad did not rescue the *sakura* mutant phenotypes.

We then tested whether overexpression of a constitutively active form of the Dpp receptor Thickveins (Tkv.Q253D) (Casanueva and Ferguson 2004) could rescue the phenotypes. Expression of *UASp-tkv.Q253D* in the germline using a *NGT-Gal4* in a control (y^{RNAi}) background resulted in 100% tumorous ovarioles, as expected (Fig. S12A). When co-expressed with *sakura* RNAi, Tkv.Q253D increased the proportion of tumorous ovarioles and decreased the proportion of germless ovarioles relative to $sakura^{RNAi}$ alone but did not restore normal ovarioles. The number of GSC-like cells was also increased by Tkv.Q253D expression in $sakura^{RNAi}$ (Fig S12B), indicating partial phenotypic modulation via BMP pathway activation.

Sakura binds Otu

To explore the molecular function of Sakura in oogenesis, we aimed to identify Sakura-interacting proteins. We conducted a co-immunoprecipitation experiment using anti-GFP magnetic beads on

377 the ovary lysates of flies expressing Sakura-EGFP, followed by mass spectrometry to identify co-
378 immunoprecipitated proteins. Ovary lysates from flies without the *sakura-EGFP* transgene
379 (*w1118*) served as negative controls. Mass spectrometric analysis revealed several proteins with
380 peptide signals present in all three biological replicates of the Sakura-EGFP samples without any
381 signals in any of the three biological replicates of the negative control (Table 1). Among these, the
382 most promising candidate, exhibiting the highest unique peptide signal in each of three replicates
383 of the Sakura-EGFP samples was Otu.

384 To confirm this finding, we generated a polyclonal anti-Otu antibody and validated it by
385 Western blots using ovary lysates from the hypomorphic otu^{14} mutant (Fig S13A) (King et al.
386 1986; Storto and King 1987; Steinhauer and Kalfayan 1992a; Pauli et al. 1993). Using this
387 antibody, we detected endogenous Otu protein in the Sakura-EGFP immunoprecipitants from
388 ovaries of 3–7-day-old flies, but not in the negative control (Fig 8A), validating the mass
389 spectrometry results. Next, using wild-type (without Sakura-EGFP) ovary lysates from 3–7-day
390 old-flies, we immunoprecipitated endogenous Sakura with anti-Sakura antibody and detected
391 endogenous Otu in the immunoprecipitant by Western blot (Fig 8B), demonstrating that
392 endogenous Sakura interacts with endogenous Otu. Furthermore, we found that ectopically
393 expressed Flag-tagged Otu co-immunoprecipitated with ectopically expressed HA-tagged Sakura
394 in S2 cells (Fig 8C).

395 The *otu* gene encodes two annotated protein isoforms, a predominant 98 kDa isoform and
396 a less abundant 104 kDa isoform generated by alternative splicing (Steinhauer and Kalfayan
397 1992b). The 98 kDa isoform lacks the Tudor domain, which is encoded by an alternatively spliced
398 126-nucleotide exon (Fig 9B. Otu(ΔTudor)) (Van Buskirk and Schupbach 2002). Previous studies
399 have shown that the 104 kDa Otu isoform is more abundant in predifferentiated germline cells and

400 is sufficient to carry all known Otu functions, whereas the 98 kDa Otu isoform becomes prominent
401 during later stages of oogenesis and is implicated in nurse cell regression and oocyte maturation
402 (Sass et al. 1995). Consistent with these findings, we observed that ovaries from very young (2–5
403 hour old) flies—containing only germaria and previtellogenic egg chambers—predominantly
404 expressed the 104 kDa isoform (Fig S13B). In contrast, ovaries from 3–7 day old flies—containing
405 all 14 stages of oogenesis—predominantly expressed the 98 kDa isoform. Importantly, both the
406 104 kDa and 98 kDa isoforms co-immunoprecipitated with endogenous Sakura using anti-Sakura
407 antibody, demonstrating that Sakura interacts with both isoforms of Otu and that the Tudor domain
408 is not required for this interaction (Fig. S13B).

409 Next, we sought to identify which regions of Sakura and Otu are important for their
410 interaction. We predicted the structure of the Sakura-Otu protein complex using AlphaFold
411 (Jumper et al. 2021; Yang et al. 2023). AlphaFold suggested that the N-terminal region of Sakura
412 (1-49aa) and the N-terminal region of Otu (1-405aa) are highly likely to form interactions, while
413 the C-terminal region of Sakura (100-144aa) does not interact with Otu (Fig 9A-C). The Tudor
414 domain of Otu is not directly involved in this interaction, consistent with our findings (Fig S13B).
415 To experimentally validate the predictions made by AlphaFold, we generated a series of truncated
416 Otu fragments, including Otu(ΔTudor) (1-336, 389-853aa, corresponding to the endogenous 98
417 kDa isoform), Otu(N1) (1-405aa), Otu(N2) (1-339aa), and Otu(C) (405-853aa) (Fig 9B). We then
418 performed co-immunoprecipitation assays to test which fragments could interact with full-length
419 Sakura. All fragments except Otu(C) were associated with full-length Sakura protein in S2 cells
420 (Fig 9D), demonstrating that the C-terminal low-complexity region of Otu is dispensable for the
421 interaction. This assay also showed that the Tudor domain is not critical and the N-terminal

422 fragment (1-339aa) of Otu is sufficient for interaction with Sakura. These findings align well with
423 the predictions made by AlphaFold.

424 Subsequently, we created several truncated Sakura fragments and conducted co-
425 immunoprecipitation assays in S2 cells to determine which Sakura fragments can interact with
426 full-length Otu. The fragments generated included Sakura(NM) (1-100aa), Sakura(NC) (1-49, 100-
427 144aa), Sakura(MC) (49-144aa), Sakura(N) (1-49aa), Sakura(M) (49-100aa), and Sakura(C) (100-
428 144aa) (Fig 9C). We found that Sakura(NM), Sakura(NC), Sakura(N), and Sakura(M) were
429 associated with Otu (Fig 9E). Compared to Sakura(NM) and Sakura(N), the interaction of
430 Sakura(M) with Otu is relatively weaker, as indicated by a fainter band in the Western blot (Fig
431 9E). Sakura-NC exhibited a weak interaction with Otu, while Sakura(MC) and Sakura(C) showed
432 no interaction (Fig 9E). These assays demonstrated that the N-terminal region (1-49aa) of Sakura
433 is sufficient for interaction with Otu. Moreover, the results suggest that the C-terminal region of
434 Sakura (100-144aa) does not interact with Otu and that adjoining it with the N-terminal (1-49aa)
435 or the middle (M) region (49-100aa) weakens the interaction with Otu. These findings support the
436 AlphaFold predictions.

437 Finally, to test whether the interaction between Sakura and Otu can be achieved solely
438 through their N-terminal regions, we performed co-immunoprecipitation assay with Sakura(N) and
439 Otu(N2). We discovered that Sakura(N) and Otu(N2) physically interact (Fig 9F). A reciprocal
440 co-immunoprecipitation assay also confirmed their interaction (Fig S14), revealing that the
441 interaction between Sakura and Otu can be established with just the 1-49aa of Sakura and the 1-
442 339aa of Otu. Therefore, we conclude that Sakura interacts with Otu *in vivo,* and the N-terminal
443 regions of both proteins are sufficient for their interaction.

444

445 **Loss of *otu* phenocopies loss of *sakura***

446 Having established the interaction between Sakura and Otu, we were interested in whether they
447 function together during oogenesis. We speculated that for them to interact and function together,
448 Sakura and Otu must exhibit similar expression and localization patterns in ovaries. We generated
449 two transgenic flies carrying full-length *otu-EGFP* or *otu(ΔTudor)-EGFP* transgenes; both
450 constructs are C-terminally fused with EGFP and under the control of the *otu* promoter. We found
451 that both Otu-EGFP and Otu(ΔTudor)-EGFP display similar expression and localization patterns
452 to Sakura-EGFP (Fig 1E, 1F and Fig 10A). Like Sakura-EGFP, Otu-EGFP and Otu(ΔTudor)-EGFP
453 are specifically expressed in germ cells, but not in follicle cells, and are localized to the cytoplasm,
454 being enriched in the developing oocytes (Fig 10A). We did not observe any difference in
455 localization patterns between Otu-EGFP and Otu(ΔTudor)-EGFP; suggesting that the Tudor
456 domain is not crucial for Otu protein localization. Notably, the localization pattern exhibited by
457 the transgenic Otu-EGFP generated in this study is consistent with a previous report (Glenn and
458 Searles 2001).

459 Previous studies have shown that mutations in *otu* lead to defects in germ cell division and
460 differentiation, resulting in phenotypes including tumorous ovarioles (King and Riley 1982; King
461 et al. 1986; Storto and King 1988; Steinhauer and Kalfayan 1992b). To study the role of *otu*
462 specifically in the germline, we performed RNAi knockdown of *otu* in the germline driven by *nos-*
463 *Gal4-VP16* (Fig 10B and 10C). Interestingly, we found that germline depletion of *otu* results in
464 rudimentary ovaries, similar to the loss of *sakura* (Fig 2C, Fig 5A, and Fig 10B). Furthermore,
465 similar to *sakura* RNAi (Fig 5), *TOsk-Gal4*-driven *otu* RNAi knockdown did not affect ovary
466 morphology (Fig 10B), but it resulted in a reduced number of eggs laid and stage 14 oocytes
467 compared with control RNAi (w^{RNAi}) (Figure 10D and 10E).

468 Given that *sakura* loss of function causes tumorous and germless ovarioles, apoptosis,
469 piRNA pathway defects, *bam* misexpression, and reduced pMad levels (Fig 3, 4 and 7A-D), we
470 asked whether similar defects occur upon *otu* depletion. Germline *otu* RNAi knockdown in 2-5
471 days old flies using *UAS-Dcr2* and *NGT-Gal4* lead to both germless (~70%) and tumorous (~30%)
472 ovarioles, closely resembling the phenotype of *sakura* RNAi (Fig S10A). Similar germless and
473 tumorous phenotypes were also observed in *nos-Gal4-VP16* > otu^{RNAi} flies (Fig 11A). In these
474 otu^{RNAi} ovarioles, Bam-GFP expression was no longer restricted to 8-cell cysts, instead persisting
475 throughout the germarium and egg chambers (Fig 11A). Additionally, $otu^{14/14}$ mutant GSCs
476 showed reduced pMad levels (Fig 11B), and cleaved Caspase-3 staining revealed elevated
477 apoptosis in *otu* RNAi ovaries (Fig 11C). Germline depletion of *otu* resulted in elevated expression
478 of GFP and β-Gal produced by the *Burdock* sensor, indicating loss of piRNA-mediated transposon
479 silencing (Fig 11D).

480 Together, these data demonstrate that *otu* loss-of-function closely phenocopies *sakura* loss-
481 of-function, including defects in germline maintenance and differentiation, *bam* misexpression,
482 reduced pMad signaling, and compromised piRNA pathway activity. These findings, along with
483 physical interaction between Sakura and Otu (Figs 8, 9, S13, and S14), suggest that they function
484 together in regulating germline maintenance and differentiation.

485 To further explore their genetic interaction, we compared the ovariole phenotypes caused
486 by single and double knockdowns of *sakura* and *otu* in the germline driven by *UAS-Dcr2* and
487 *NGT-Gal4*. Individual knockdown of either gene resulted in ~70% germless and ~30% tumorous
488 ovarioles in 2-5 days old flies (Fig S10A). Simultaneous knockdown of both genes increased the
489 propotion of germless ovarioles to 86%, with a corresponding decrease in tumorous phenotypes to
490 14%, suggesting a synergistic enhancement of the germless phenotype. The number of GSC-like

491 cells were not affected by the double knockdown of *sakura* and *otu* compared with their respective
492 single knockdown (Fig S10B).

493

494 **Sakura and Otu proteins do not depend on each other for their abundance**

495 We investigated whether Sakura and Otu proteins depend on each other for their abundance. We
496 performed Western blot analysis on ovaries with germline-specific knockdown of *sakura* or *otu*,
497 driven by *TOsk-Gal4*. Otu protein levels were not reduced in $sakura^{RNAi}$ ovaries compared to
498 control y^{RNAi} (Fig S15A), and conversely, Sakura levels were not decreased in otu^{RNAi} ovaries
499 compared with control w^{RNAi} ovaries (Fig S15B). These results indicate that Sakura and Otu do not
500 require each other for their protein expression or stability.

501 To further test this conclusion and to examine whether Otu enrichment to the posterior of
502 egg chambers is affected by loss of *sakura*, we generated marked $sakura^{null}$ germline clones using
503 the FLP-FRT system. Clones were marked by the absence of RFP, and experiments were performed
504 in the flies expressing the *otu-EGFP* or *otu(ΔTudor)-EGFP* transgene in an otherwise wild-type
505 ($otu^{+/+}$) background. Otu-EGFP fluorescence signal was comparable between $sakura^{null}$ clones
506 (*FRT82B*, $sakura^{null}$) and control clones (*FRT82B*) (Fig 12A). Similarly, Otu(ΔTudor)-EGFP levels
507 were unaffected in $sakura^{null}$ clones compared to the control clones (Fig 12B), confirming that
508 Sakura is not required for Otu protein expression or stability.

509 Both Otu-EGFP and Otu(ΔTudor)-EGFP exhibited clear enrichment at the posterior of egg
510 chambers in the control clones (*FRT82B*) —consistent with localization to the developing oocyte
511 (Fig 12A and 12B). This posterior enrichment was absent in $sakura^{null}$ clones, demonstrating that
512 Sakura is crucial for this process.

513

514 **Sakura does not affect Otu's deubiquitinase activity in vitro**

515 A previous study has shown that Otu possesses deubiquitinase activity (Ji et al. 2017). We asked
516 whether Sakura regulates the Otu's deubiquitinase activity. To test this, we performed an in vitro
517 deubiquitination assay using Ub-Rhodamine 110 as a model substrate. Consistent with the
518 previous study (Ji et al. 2017), we detected a deubiquitinase activity in Otu that was ectopically
519 expressed and purified from S2 cells (Fig S16). The presence of Sakura, purified from *E.coli,* did
520 not affect Otu's deubiquitinase activity under these assay conditions. Additionally, Sakura itself
521 did not exhibit deubiquitinase activity.

522

523 **Discussion**

524 In this study, we identified Sakura, encoded by a previously uncharacterized gene *CG14545*, as an
525 essential factor for oogenesis and female fertility. We demonstrated that Sakura is specifically
526 expressed in germline cells in the ovary, including GSCs, is localized to the cytoplasm, and is
527 enriched in the developing oocytes. *sakura* homozygous null mutant flies are viable but completely
528 female-sterile and male-fertile. Loss of *sakura*, either through null mutation or germline RNAi
529 including in GSCs, results in rudimentary ovaries exhibiting germless and tumorous phenotypes.

530 The tumorous phenotype associated with the loss of *sakura* is characterized by an excess
531 of GSC-like cells, which feature round spectrosomes, as well as cyst cells with branched fusomes
532 (Fig 3C). The increased number of GSC-like cells in loss of *sakura* suggests dysregulation of GSC
533 self-renewal and differentiation. Meanwhile, the presence of excess cyst cells with branched
534 fusomes indicates abnormal differentiation and division of cysts. Differentiation of cystoblasts

535 typically involves four mitotic divisions with incomplete cytokinesis, leading to 16 cyst cells
536 interconnected by branched fusomes. The degree of fusome branching serves as a marker for the
537 stages of cyst cell division, with increased branching from 2-cell to 16-cell cysts (de Cuevas and
538 Spradling 1998). Notably, fusomes begin to degenerate and disappear after 16-cell cysts as the
539 germline cyst enters the meiotic zone or region 2 of the germarium. The persistence of cyst cells
540 with branched fusomes in *sakura*$^{null/null}$ suggests that *sakura* is crucial for the proper division and
541 differentiation of cysts, and we speculate that it is required for germline cysts to enter meiotic
542 division.

543 Mosaic analysis of *sakura*^{null} indicates that *sakura* is intrinsically required for the
544 establishment of GSCs in the ovary. When mutant clones were induced in PGC stage, significantly
545 fewer *sakura*^{null} marked GSCs were observed in adult ovaries, suggesting that many *sakura*^{null}
546 PGCs fail to survive or differentiate into GSCs. Furthermore, induction of *sakura*^{null} clones in adult
547 ovaries led to a more rapid decline in marked *sakura*^{null} GSCs compared to controls, indicating
548 that *sakura* is also intrinsically required for GSC maintenance (Fig 6A). Over time, germaria
549 containing *sakura*^{null} GSC clones became increasingly tumorous, with an expanding population of
550 *sakura*^{null} GSC-like cells (Fig 6B and 6C). In contrast, the number of GSC-like cells across entire
551 and all ovarioles regardless of whether GSCs in the niche remain, declined over time in *sakura*^{null}
552 ovaries (Fig S5B). These results suggest that *sakura*^{null} GSCs initially undergo aberrant
553 proliferation, leading to tumor formation, but are ultimately *sakura*^{null} GSCs and GSC-like cells
554 are lost through a cell death mechanism, as evidenced by the elevated levels of cleaved Caspase-3
555 in *sakura*^{null} ovaries (Fig 3F).

556 Dpp/BMP signaling governs GSC self-renewal and cystoblast differentiation by repressing
557 *bam* in GSCs and de-repressing it in daughter cystoblasts (Fig S1). This process is mediated by the

558 transcription factor Mad, which, when phosphorylated (pMad), translocates into the nucleus to
559 repress *bam* transcription (Kirilly and Xie 2007; Kahney et al. 2019; Hinnant et al. 2020). Our
560 findings indicate that Bam expression is not limited to 8-cell cysts but continues throughout the
561 germarium in ovaries lacking *sakura* function (Fig 7A and 7B). The misexpression of Bam in
562 GSCs likely results from reduced levels of pMad in the GSCs (Fig 7C, and 7D). Given the low
563 pMad levels observed upon loss of *sakura*, we propose that *bam* misregulation in GSCs occurs
564 primarily at the transcriptional level, although Bam is also known to be subject to post-
565 transcriptional regulation (Pek et al. 2009). The continued expression of Bam throughout the
566 germarium, well beyond the GSC niche, suggests a failure to terminate *bam* expression at the 16-
567 cell cyst stage —a developmental transition when *bam* is normally turned off. Thus, *sakura*
568 mutants likely exhibit two distinct molecular defects contributing *bam* overexpression: (1)
569 impaired Dpp/BMP signaling within the GSC niche, and (2) a failure to downregulate *bam* at 16-
570 cell stage. Given the limited space within the GSC niche, the latter defect may be the predominant
571 contributor to the observed *bam* overexpression. The molecular mechanism that silences *bam* at
572 the 16-cell cyst stage remains poorly understood, and how *sakura* loss perturbs this regulation is
573 unclear. The *sakura* mutant may therefore serve as a valuable model to investigate the mechanism
574 that normally suppresses *bam* expression at the 16-cell stage.

575 Transposons are mobile genetic elements that, if not silenced, can generate DNA damage
576 and genomic instability (Levin and Moran 2011). piRNAs derived from transposons and other
577 repeats can target and silence transposon RNAs to preserve genome integrity in germ cells (Siomi
578 et al. 2011). Loss of piRNAs leads to transposon derepression, resulting in increased DNA damage,
579 which subsequently triggers cell death (Kang et al. 2018; Moon et al. 2018). Genetic damage in
580 germ cells can cause developmental defects and diseases that may be inherited by the next

581 generation. Thus, elimination of defective germ cells is crucial for maintaining germline integrity
582 of a species (Chu et al. 2014; Ota and Kobayashi 2020). We found that loss of *sakura* results in
583 reduced piRNA levels and loss of piRNA-mediated transposon silencing in the germline (Fig 4).
584 The observed apoptosis, indicated by elevated cleaved Caspase-3 levels in *sakura* mutant ovaries
585 (Fig 3F), suggest that desilencing of transposon due to reduced piRNA levels likely results in
586 increased DNA damage, triggering cell death. We speculate that the germless phenotype in *sakura*
587 mutants may partly arise from an apoptotic germline elimination program activated to maintain
588 germline integrity.

589 In addition to its expression in GSCs and cysts in the germarium, Sakura is also expressed
590 in germline cells in later-stage egg chambers (Fig 1E-F) and is required at this stage for proper
591 oogenesis. When Sakura is depleted from region 2b of the germarium onward —leaving GSCs and
592 early cyst cells intact—females have significantly fewer stage 14 oocytes and lay significantly
593 fewer eggs (Fig 5). The failure to produce stage 14 mature oocytes likely stems from cytoskeletal
594 disorganization that disrupt oocyte development, as evidenced by mislocalization of Orb (Fig 5E,
595 S7, and S12). Notably, piRNA pathway mutants also exhibit similar Orb mislocalization (Ohtani
596 et al. 2013). Therefore, the reduced piRNA levels (Fig 4) may contribute to the oocyte development
597 defects, including Orb mislocalization, in *sakura* mutants. (Fig 5E).

598 Sakura does not possess any known protein domains. To infer its function, we identified
599 Otu, a protein known to be crucial for oogenesis, as a protein partner of Sakura. Mutations in *otu*
600 gene lead to a range of ovarian phenotypes, including germ cell loss, tumorous egg chambers filled
601 with undifferentiated germ cells, defects in germlne sexual identity determination, abnormalities
602 in nurse cell chromosome structure, and defects in oocyte determination (King and Riley 1982;
603 Storto and King 1988; Pauli et al. 1993; Glenn and Searles 2001). We showed that germline

604 depletion of Otu via RNAi phenocopies loss of *sakura*. Similar to Sakura, loss of *otu* inhibits
605 Dpp/BMP signaling, resulting in low pMad levels in GSCs and Bam de-repression (Fig 11A-B).
606 Additionally, loss of *otu* also results in the loss of piRNA-mediated silencing, paralleling the
607 effects of *sakura* loss. Furthermore, germline knockdown of *otu* yielded a similar ratio of germless
608 ovaries as seen in *sakura-RNAi,* and simultaneous knockdown of both *otu* and *sakura* exacerbated
609 the germless ovary phenotype (Fig S10). These observations raise the possibility that Sakura and
610 Otu function together to regulate germ cell maintenance in the ovaries and are involved in
611 Dpp/BMP signaling to balance stem cell renewal and differentiation.

612 Otu possesses deubiquitinase activity, catalyzed by its N-terminal Otu domain (Ji et al.
613 2017; Ji et al. 2019). In germ cells, Otu interacts with Bam, forming a deubiquitinase complex that
614 deubiquitinates and thereby stabilizes CycA, promoting GSC differentiation. The predicted
615 structure of Sakura and Otu complex suggests that the Mid domain of Sakura directly contacts the
616 Otu domain of Otu (Fig 9A). We found that Sakura lacks a deubiquitinase activity and it does not
617 directly affect Otu's deubiquitinase rate in our in vitro assays using Ub-Rhodamine 110 as a
618 substrate (Fig S16). This does not preclude the possibility that Sakura may still influence Otu's
619 deubiquitinase activity, potentially guiding Otu to its substrate and determining substrate
620 specificity. Our in vitro assays may not have detected such specificity changes.

621 Otu is an RNA-binding protein whose deubiquitinase activity is enhanced by RNA binding
622 (Ji et al. 2019). Bam, along with other proteins such as Bgcn, Mei-P26, and Sxl, binds —a key
623 stem cell maintenance factor (Wang and Lin 2004)— and represses its translation in GSCs (Wang
624 and Lin 2004; Li et al. 2009; Chau et al. 2012; Li et al. 2013). Bam and Otu form a protein complex
625 (Ji et al. 2017). Future studies should explore whether Sakura modulates Otu's RNA-binding
626 properties and its interaction with other proteins. Although Sakura is exclusively expressed in

627 ovaries, particularly in germline cells including GSCs (Fig 1), Otu is broadly expressed in various
628 tissues, including testes and gut (Steinhauer and Kalfayan 1992b). This restricted expression
629 pattern suggests that Sakura may serve as a female germline-specific cofactor that enhances or
630 modifies Otu's molecular functions. Identifying Otu's RNA targets and deubiquitinase substrates
631 beyond CycA, as well as determining how Sakura binding influences these activities, will be key
632 to elucidating their roles in oogenesis. One intriguing possibility is that Sakura regulates Otu's
633 activity toward piRNA pathway components, thereby contributing proper piRNA biogenesis and
634 function. Additionally, the Sakura-Otu complex may directly regulate essential post-transcriptional
635 processes such as *sxl* alternative splicing and translational control of other oogenic RNAs.

636 In summary, this study identifies and characterizes the previously unknown gene *sakura*,
637 which is specifically expressed in female germ cells and is essential for oogenesis and female
638 fertility. Together with its protein partner Otu, Sakura likely regulates germline cell fate,
639 maintenance, and differentiation.

640

641 **Materials and Methods**

642 **Fly strains**

643 We generated the *sakura*^{null} strain by introducing indels within the Sakura coding region using the
644 CRISPR/Cas9 genome editing system, as we previously reported (Zhu et al. 2018a; Zhu et al.
645 2018b; Zhu et al. 2019b; Zhu and Fukunaga 2021). The transgenic *sakura-EGFP, otu-EGFP,* and
646 *otu(ΔTudor)-EGFP* strains were created following previously published methods (Fukunaga et al.
647 2012; Kandasamy and Fukunaga 2016; Zhu and Fukunaga 2021). A fragment containing Sakura
648 cDNA flanked by ~1 kbp upstream and ~1 kbp downstream genomic sequences was cloned.

649 Fragments containing Otu and Otu(ΔTudor) cDNAs, flanked by ~2.5 kbp upstream and ~1 kbp
650 downstream genomic sequences, were also cloned. The EGFP gene was fused in-frame to the C-
651 terminus of the Sakura and Otu coding sequences within these fragments, which were then inserted
652 into a pattB plasmid vector. The *sakura-EGFP* plasmid was integrated into the 51C1 site within
653 the fly genome using the BDSC:24482 fly strain and the PhiC31 system, while the *otu-EGFP* and
654 *otu(ΔTudor)-EGFP* plasmids were integrated into the 25C6 site of the genome using the attP40 fly
655 strain and the PhiC31 system.

656 The *sakura RNAi* #1 (VDRC: v39727) and #2 (VDRC: v103660), *y-RNAi* (v106068),
657 *TOsk-Gal4* (v 314033), Burdock sensor [*UAS-Dcr2; NGT-Gal4; nosGal4-VP16,*
658 *nos>NLS_GF'_lacZ_vas-3'UTR_burdock-target*] (v 313217) strains were from Vienna
659 *Drosophila* Resource Center. *w-RNAi* (BDSC: 35573), *otu-RNAi* (BDSC: 34065), *bam-RNAi*
660 (BDSC: 33631), *cycA-RNAi* (BDSC: 29313), *UAS-Dcr-2; NGT-Gal4* (BDSC: 25751),
661 *FRT82B/TM6C, Sb* (BDSC: 86313), otu^{14} (BDSC: 6025), *UASp-Mad-GFP* (BDSC: 604592), and
662 *UASp-tkv.Q253D* (BDSC: 604934) were obtained from the Bloomington Stock Center. The *bam-*
663 *GFP* reporter (DGRC: 118177) and *vasa-EGFP* knocked-in fly (DGRC: 118616) were from Kyoto
664 *Drosophila* Stock Center.

665

666 **Fertility assay**

667 The female fertility assay was performed as previously described (Zhu et al. 2018b; Liao et al.
668 2019; Zhu et al. 2019a; Zhu and Fukunaga 2021). Briefly, five test virgin females of each test
669 genotype were mated with three wild-type (OregonR) males in a cage with a 6-cm grape juice agar
670 plate supplemented with wet yeast paste. The agar plates were replaced daily, and the number of

671 eggs laid on the third plate (on day 3) was recorded. After incubation at 25°C for an additional day,
672 the number of hatched eggs was counted. At least three cages per genotype were tested.

673 For the male fertility assay, a single test male was mated with five wild-type (OregonR) virgin
674 females in each vial, following previously published methods (Zhu et al. 2018b; Zhu et al. 2019a;
675 Zhu and Fukunaga 2021). After 3 days, the females were transferred to a new vial (vial 1). Every
676 two days, they were transferred to a new vial until a total of four vials were obtained. After 2 days
677 in the fourth vial, the females were removed, and the total number of progenies emerging from
678 these four vials was counted. At least five males per genotype were tested.

679

680 **Sakura and Otu antibodies**

681 We expressed a recombinant full-length Sakura protein as an N-terminal 6xHis-tagged protein in
682 *E. coli* using a modified pET vector and purified it using Ni-sepharose (GE Healthcare) and
683 HiTrapQ HP (GE Healthcare) columns (Fukunaga and Doudna 2009). Recombinant Otu fragments
684 (145-405aa and 406-853aa) were similarly expressed as N-terminally 6xHis-MBP-fusion proteins
685 in *E. coli* and purified using Ni-sepharose. These purified proteins were used as antigens to
686 generate polyclonal anti-Sakura and anti-Otu sera in rabbits (Pocono Rabbit Farm & Laboratory,
687 Inc.). The rabbit polyclonal anti-Sakura antibodies were affinity purified using His-MBP-Sakura
688 recombinant protein and Affigel-15 (Bio-rad), following the manufacturer's instructions. Rabbit
689 anti-Otu sera were first pre-cleared with purified His-MBP protein bound to Affigel-15, and the
690 unbound fraction was affinity purified using purified His-MBP-Otu fragments (145-405aa and
691 406-853aa) and Affigel-15.

692

693 **Immunostaining**

694 Stereomicroscope images of dissected ovaries were taken using Leica M125 stereomicrocsope.
695 Ovaries from 2- to 5-day-old, yeast-fed females were hand-dissected in 1X PBS (137 mM NaCl,
696 2.7 mM KCl, 10 mM Na_2HPO_4, 1.8 mM KH_2PO_4, pH 7.4) at room temperature. The dissected
697 ovaries were fixed in a fixative buffer (4% formaldehyde, 15 mM PIPES (pH 7.0), 80 mM KCl,
698 20 mM $NaCl_2$, 2 mM EDTA, and 0.5 mM EGTA), incubated for 30 minutes at room temperature
699 with gentle rocking. After fixation, the ovaries were rinsed three times with PBX (0.1% Triton X-
700 100 in 1X PBS) and then incubated in a blocking buffer (2% donkey serum in 3% BSA [w/v],
701 0.02% NAN_3 [w/v] in PBX) for 1 hour at room temperature. Then, the ovaries were incubated with
702 primary antibodies diluted in the blocking buffer overnight at 4°C. The following day, the ovaries
703 were rinsed three times with PBX and incubated with Alexa Fluor-conjugated secondary
704 antibodies for 2 hours. The ovaries were rinsed three times with PBX and then mounted in
705 VECTASHIELD® PLUS antifade mounting medium with DAPI (H-2000, Vector lab). Confocal
706 images were acquired on a Zeiss LSM700 confocal microscope at the Johns Hopkins University
707 School of Medicine Microscope Facility.

708 The primary antibodies used for immunostaining were mouse anti-HTS (1B1) (DSHB,
709 AB_528070, dilution: 1/100), mouse anti-Bam (DSHB, AB_10570327, 1/20), mouse anti-CycA
710 (DSHB, AB_528188, 1/100), rat anti-Vasa (DSHB, AB_760351, 1/100), rat anti-DE Cadherin
711 (DCAD2) (DSHB, AB_528120, 1/20), rabbit anti-pMad (Cell Signaling, Phospho-SMAD1/5
712 (Ser463/465) mAb #9516, 1/200,), and rabbit anti-cleaved caspase-3 (Cell Signaling, Cleaved
713 Caspase-3 (Asp175) #9661, 1/200). Secondary antibodies used were Alexa Fluor 488 Donkey anti-
714 Mouse Igg (ThermoFisher, A21202, 1/100), Alexa Fluor 594 Donkey anti-Rat Igg (ThermoFisher,
715 A21209, 1/100), Alexa Fluor 594 Donkey anti-Mouse Igg (ThermoFisher, A21203, 1/100), and

716 Alexa Fluor 594 Donkey anti-Rabbit Igg ThermoFisher, A21207, 1/100). Rhodamine phalloidin
717 (ThermoFisher, R415, 1/100) was used to stain F-Actin.

718

719 **Germline clonal analysis**

720 We generated *sakura*^{null} mutant clones using FLP/FRT-mediated recombination (Rubin and Huynh
721 2015). To induce *sakura*^{null} GSC clones, 3-day-old female flies of the genotype *hs-flp*/*w*; *+;*
722 *FRT82B, ubi-GFP/FRT82B, sakura*^{null} were heat-shocked at 37°C for 1 hour, twice daily, with an
723 8-hour interval between heat shocks. Female flies of the genotype *hs-flp*/*w*; +; *FRT82B, ubi-*
724 *GFP/FRT82B* were used as controls. Ovaries were dissected and stained 4, 7, and 14 days after
725 clone induction. To induce primordial germ cell (PGC) clones, early third-instar larvae were
726 subjected to the same heat shock regime, then allowed to develop to adulthood. Ovaries were
727 dissected and analyzed at 3 to 4 days after eclosion.

728 To induce *sakura*^{null} mutant clones in the presence of *otu-EGFP* or *otu(*Δ*Tudor)-EGFP*
729 transgenes, 3-day-old female flies with the genotype *hs-flp*/*w*; *otu-EGFP*/+; *FRT82B*, *ubi-*
730 *RFP*/*FRT82B*, *sakura*^{null} and *hs-flp*/*w*; *otu(ΔTudor)-EGFP* /+; *FRT82B*, *ubi-*
731 *RFP*/*FRT82B*, *sakura*^{null} were heat-shocked under the same conditions. Control genotypes were
732 *hs-flp*/*w*; *otu-EGFP*/+; *FRT82B*, *ubi-RFP*/*FRT82B* and *hs-flp*/*w*; *otu(ΔTudor)-*
733 *EGFP*/+; *FRT82B*, *ubi-RFP*/*FRT82B* were used as controls. Flies were dissected 3-4 days after
734 clone induction.

735

736

737 **Western blot**

738 Lysates of hand-dissected ovaries and tissues were prepared by homogenizing in RIPA buffer (50
739 mM Tris-HCl [pH 7.4], 150 mM NaCl, 1% [v/v] IGEPAL CA-630, 0.1% [w/v] sodium dodecyl
740 sulfate (SDS), 0.5% [w/v] sodium deoxycholate, 1 mM ethylenediaminetetraacetic acid (EDTA),
741 5 mM dithiothreitol, and 0.5 mM phenylmethylsulfonyl fluoride (PMSF)) (Kandasamy et al. 2017;
742 Zhu et al. 2018b). The homogenates were centrifuged at 21,000g at 4°C for 10 min, and the protein
743 concentration of the supernatant was determined using the BCA protein assay kit (Pierce) as
744 needed. Fifteen μg of total protein was loaded per lane for Western blot. The sources and dilutions
745 of the primary antibodies were as below. Rabbit anti-Sakura (1/10000, generated in this study),
746 rabbit anti-Otu (1/10000, generated in this study), rabbit anti-alpha-Tubulin [EP1332Y] (1/10000,
747 Abcam, ab52866), mouse anti-alpha-Tubulin [12G10] (1/10000, DSHB, AB_1157911), mouse
748 anti-FLAG (1/10000, Sigma, F1804), mouse anti-HA (1/10000, Sigma, H3663), and mouse anti-
749 GFP [GF28R] (1/3000, Invitrogen, 14-6674-82). IRDye 800CW goat anti-mouse IgG, IRDye
750 800CW goat anti-rabbit IgG, IRDye 680RD goat anti-mouse, and IgG IRDye 680RD goat anti-
751 rabbit were used as secondary antibodies. The membranes were scanned using the Li-Cor Odyssey
752 CLx Imaging System.

753

754 **Mass spectrometry**

755 Immunoprecipitation of Sakura-EGFP protein was performed using the GFP-Trap Magnetic
756 Agarose Kit (Proteintech, gtmak-20) on dissected ovaries from flies harboring *sakura-EGFP*
757 transgene, with *w1118* flies as controls. Ovaries were homogenized in 200 μL ice-cold lysis buffer
758 (10 mM Tris-HCl [pH 7.5], 150 mM NaCl, 0.5 mM EDTA, 0.05% [v/v] IGEPAL CA-630)

759 containing 1× protease inhibitor cocktail (100× protease inhibitor cocktail contains 120 mg/ml
760 1 mM 4-(2-aminoethyl) benzene sulfonyl fluoride hydrochloride (AEBSF), 1 mg/ml aprotinin,
761 7 mg/ml bestatin, 1.8 mg/ml E-64, and 2.4 mg/ml leupeptin). After homogenization, the tubes were
762 placed on ice for 30 minutes, and the homogenates were extensively pipetted every 10 minutes.
763 The lysates were then centrifuged at 17,000x g for 10 minutes at 4°C. The supernatants were
764 transferred to pre-chilled tubes, and 300 µL dilution buffer (10 mM Tris/Cl pH 7.5, 150 mM NaCl,
765 0.5 mM EDTA) supplemented with 1x protease inhibitor cocktail were added. The diluted lysates
766 were then added to the GFP-trap magnetic beads in 1.5 mL tubes and rotated for 1 hour at 4°C.
767 After separating the beads with a magnetic tube rack, the beads were washed three times with 500
768 µL wash buffer (10 mM Tris/Cl pH 7.5, 150 mM NaCl, 0.05 % [v/v] IGEPAL CA-630). Proteins
769 were eluted with 40 µL acidic elution buffer (200 mM glycine pH 2.5) followed by immediate
770 neutralization with 5 uL neutralization buffer (1 M Tris pH 10.4).

771 As a quality control before mass spectrometry, ~5 µL of the samples were mixed with an
772 equal volume of 2× SDS-PAGE loading buffer (80 mM Tris-HCl [pH 6.8], 2% [w/v] SDS, 10%
773 [v/v] glycerol, 0.0006% [w/v] bromophenol blue, 2% [v/v] 2-mercaptoethanol), heated at 95 °C
774 for 3 min, and run on 4–20% Mini-PROTEAN® TGX™ Precast Protein Gels (Biorad, #4561094).
775 Silver staining was then performed by using Pierce™ Silver Stain Kit (ThermoFisher, 24612) to
776 assess the quality of the immunoprecipitated protein samples. Mass spectrometry was conducted
777 at the Mass Spectrometry Core at the Department of Biological Chemistry, Johns Hopkins School
778 of Medicine, as previously described (Zhu and Fukunaga 2021).

779

780 **Co-immunoprecipitation**

781 For co-immunoprecipitation of endogenous Sakura protein, wild-type ovaries (*w1118*) were
782 homogenized in RIPA buffer, centrifuged at 21,000g at 4°C for 10 min, and the clear supernatant
783 protein lysates were used for immunoprecipitation. Four μg of rabbit anti-Sakura and normal rabbit
784 IgG (Cell Signaling, #2729) were incubated with 50 μL of Dynabeads Protein G (ThermoFisher,
785 10004D) for 20 min at room temperature. The beads were washed once with PBST (1x PBS with
786 0.1% Tween-20). The ovary lysate supernatant was then incubated with the washed beads at room
787 temperature for 30 min, followed by three washes with PBST. The proteins were eluted with 2x
788 SDS-PAGE loading buffer (80 mM Tris-HCl [pH 6.8], 2% [w/v] SDS, 10% [v/v] glycerol,
789 0.0006% [w/v] bromophenol blue, 2% [v/v] 2-mercaptoethanol) and heated at 70°C for 10 min.
790 After bead separation using a magnetic tube rack, the eluted proteins in 2x SDS-PAGE loading
791 buffer were heated again at 95°C for 3 min.

792 Transient protein expression in S2 cells was performed using the pAc5.1/V5-HisB plasmid
793 vector (Invitrogen). A total of 1 μg plasmids were transfected using the Effectene transfection
794 reagent (Qiagen, 301425). Three days after transfection, cells were harvested and lysed with ice-
795 cold lysis buffer supplemented with 1× protease inhibitor cocktail. The cell lysates were then
796 centrifuged at 17,000x g for 10 min at 4°C, and the clear supernatants were collected for
797 immunoprecipitation. For anti-HA immunoprecipitation, supernatants were incubated with 25 μL
798 (0.25 mg) of Pierce™ Anti-HA Magnetic Beads (ThermoFisher, 88837) at room temperature for
799 30 min. The beads were then washed three times with TBST (1x TBS [0.05 M Tris/HCl and 0.15
800 M NaCl, pH 7.6] with 0.05% Tween-20). For anti-FLAG immunoprecipitation, 2 μg of mouse anti-
801 FLAG (1/10000, Sigma, F1804) was incubated with 50 μL of Dynabeads Protein G
802 (ThermoFisher, 10004D) for 10 min at room temperature. The beads were washed once with
803 PBST. The S2 cell lysate supernatant was incubated with the washed beads at room temperature

804 for 15 min. The beads were washed three times with PBST. In both anti-HA and anti-FLAG
805 immunoprecipitations, proteins were eluted with 2× SDS-PAGE loading buffer. For anti-HA, the
806 beads in 2x SDS-PAGE loading buffer were heated at 95°C for 7 min. For anti-FLAG, the beads
807 were heated at 70°C for 10 min, then were separated using a magnetic tube rack. The eluted
808 proteins in 2x SDS-PAGE loading buffer were heated again at 95°C for 3 min.

809

810 **Small RNA and mRNA sequencing**

811 Poly-A+ mRNA purification was performed as previously described (Fukunaga et al. 2012). Small
812 RNA libraries and poly-A+ mRNA libraries were prepared, sequenced on Hiseq2500 (Illumina),
813 and analyzed, as previously reported (Fukunaga et al. 2014; Kandasamy et al. 2017; Liao et al.
814 2018; Zhu et al. 2018a; Zhu et al. 2018b; Liao et al. 2019; Zhu et al. 2019a; Zhu et al. 2019b).
815 SRA accession number for these datasets is PRJNA1156618.

816

817 **RT-PCR**

818 Total RNAs from testes and ovaries were prepared using miRVana (Thermo Fisher Scientific).
819 RNAs were treated with Turbo DNase (Thermo Fisher Scientific) to remove potential genomic
820 DNA contamination. A total of 1 μg of RNA was reverse-transcribed into cDNA using
821 SuperScript™ VILO™ MasterMix (Thermo Fisher Scientific). To assess *sxl* alternative splicing,
822 PCR was performed using GoTaq Green Master Mix (Promega) with the primers *sxl*-F
823 (CTCACCTTCGATCGAGGGTGTA) and *sxl*-R (GATGGCAGAGAATGGGAC).

824

825 **In vitro deubiquitination assay**

826 C-terminally 6xHis-tagged recombinant Sakura protein was expressed in *E. coli* using a modified
827 pET vector and was purified using Ni-sepharose. N-terminally 3xHA-HRV3Csite-3xFLAG-
828 tagged Otu protein and a negative control, N-terminally 3xHA-HRV3Csite-3xFLAG-tagged
829 firefly luciferase protein, were expressed in S2 cells using pAc5.1/V5-HisB vector. The proteins
830 were immunoprecipitated using Pierce™ Anti-HA Magnetic Beads (ThermoFisher, 88837) as
831 described previously, with a more stringent washing step to effectively remove interacting proteins.
832 The beads were washed six times with a high salt wash buffer (TBST with 800 mM NaCl). The
833 proteins were eluted by cleaving off 3xHA tag with 25 nM GST-HRV3C protease in a cleavage
834 buffer (25mM Tris-HCl pH 7.4, 150 mM NaCl, 5% glycerol, 2mM EDTA), incubated at 4°C with
835 rotation for 6 hours. An equal volume of 100% glycerol was added to the eluted protein.

836 Purified proteins, including Otu, luciferase, and Sakura, were mixed with Ub-Rhodamine
837 110 (Ubiquitin-Proteasome Biotechnologies, M3020) in a total volume of 30 μL in reaction buffer
838 (20 mM Tris-HCl, pH 7.5, 200 mM NaCl, 5 mM $MgCl_2$, 2 mM DTT). The mixture was added to
839 a black 384-well low-volume plate. Fluorescence measurements were taken using SpectraMax i3x
840 Multi-Mode Microplate Reader at 37°C, with excitation and emission wavelengths set at 485/20
841 and 530/20 nm respectively. The fluorescence intensity for each condition was averaged from
842 triplicates and plotted as a function of time.

843

844 **Acknowledgments**

845 We thank Bloomington Drosophila Stock Center, Vienna Drosophila Resource Center, and Kyoto
846 Drosophila Stock Center for fly strain stocks. We thank the Johns Hopkins University School of

847 Medicine Microscope Facility for use of the Zeiss LSM700, supported by NIH grant
848 S10OD016374 awarded to Dr. Scot C. Kuo. We thank Ms. Lauren DeVine and Dr. Bob Cole at the
849 Johns Hopkins University School of Medicine Mass Spectrometry and Proteomics Core Facility
850 for the mass-spec analysis. This work was supported by the grants from the National Institutes of
851 Health [R35GM145352 and R03AI178064] and Johns Hopkins University Catalyst Award to RF.

852

853 **Author Contributions**

854 Methodology and Investigation, A.A., L.Z., and R.F.; Conceptualization and Writing, A.A. and
855 R.F.; Funding Acquisition and Supervision, R.F.

856

857 **Competing interests**

858 The authors have no conflicts of interest to declare.

859

860 **Figure Legends**

861 **Fig 1. Sakura expression pattern and mutant allele**

862 (A) Schematic illustration of *Drosophila* ovary and germarium. *Drosophila* female has a pair of
863 ovaries, each consisting of 12-16 ovarioles (cyan). The germarium (outlined with magenta) is
864 located at the anterior tip of the ovarioles and consists of both germ cells and somatic cells. Germ
865 cells include germline stem cells (GSCs), cystoblasts, cysts, and differentiating oocytes. Somatic
866 cells include terminal filament (TF) cells, cap cells (CCc), escort cells (ECs), and follicle cells

867 (FCs). GSCs and cystoblasts have spherical, unbranched spectrosomes, whereas cysts posesss
868 branched fusomes. The distinct regions of the germarium—1, 2a, 2b, and 3—are indicated. (B)
869 *Drosophila* Sakura protein (Sakura/CG14545) and its null mutant allele generated in this study.
870 (C) Western blot of dissected fly tissues. (D) Western blot of ovary lysates. (E) Confocal images
871 of the germarium from the *sakura-EGFP* transgenic fly. Sakura-EGFP (green), Hts (red), and
872 DAPI (blue). Scale bar: 10 μm. (F) Confocal images of the egg chambers from the *sakura-EGFP*
873 transgenic fly. Sakura-EGFP (green), Vasa (red), and DAPI (blue). Sakura-EGFP is expressed in
874 nurse cells and enriched in the developing oocyte (yellow arrow). Scale bar: 20 μm.

875

876 **Fig 2. *sakura* mutant flies are female-sterile and have rudimentary ovaries.**

877 (A-B) Female fertility assays. (A) The number of eggs laid by test females crossed with OregonR
878 wild-type males and (B) hatching rates of the eggs. Mean ± SD (n = 3). P-value < 0.001 (Student's
879 t-test, unpaired, two-tailed) is indicated by ***. (C) Stereomicroscope images of dissected whole
880 ovaries. Scale bar: 200 μm.

881

882 **Fig 3. *sakura*^{null} ovaries are germless and tumorous**

883 (A, B) Confocal images of the ovaries from control (*sakura*$^{null/+}$) and *sakura*$^{null/null}$ expressing Vasa-
884 EGFP. Vasa-EGFP (green) and DAPI (blue). Yellow stars indicate the anterior tip of normal
885 ovarioles, while orange and cyan stars indicate the anterior tips of tumorous and germless
886 ovarioles, respectively, in Figure 1. Higher-magnification images of the germarium regions are
887 shown in (B). Scale bars: 10 μm for (A) and 50 μm for (B). (C) Confocal images of control
888 (*sakura*$^{null/+}$) and *sakura*$^{null/null}$ ovaries stained with anti-Hts antibody to label spectrosomes and

889 fusomes. Hts (red) and DAPI (blue). Yellow, orange, and cyan dotted lines mark the normal,
890 tumorous, germless and germaria, respectively. Scale bars: 10 μm. (D) Ratio (%) of normal,
891 germless, and tumorous ovarioles of indicated genotypes (ages 2-5 days; n=33, 25, 74, 29
892 respectively). (E) Quantification of GSC-like cell number per germarium in the indicated
893 genotypes (ages 2-5 days; n = 33, 30, 35, and 31 respectively). (F) Confocal images of control
894 (*sakura*$^{null/+}$) and *sakura*$^{null/null}$ ovaries stained with anti-cleaved Caspase-3 antibody. Cleaved
895 caspase-3 (red) and DAPI (blue). Scale bars: 20 μm.

896

897 **Fig 4. Loss of *sakura* results in lower piRNA levels and loss of piRNA-mediated transposon**
898 **silencing**

899 (A) Scatter plots of normalized number of transposon piRNA reads from small RNA-seq of
900 indicated genotypes compared with *sakura*$^{+/+}$. Means of three biological replicates are plotted.
901 Downregulated (fold-change < 0.5) and upregulated (fold-change > 2) transposon piRNAs are
902 shown in cyan and magenta, respectively. (B) Volcano plots of transposon RNAs from RNA-seq
903 of indicated genotypes compared with *sakura*$^{+/+}$. Three biological replicates per genotype were
904 analyzed. Downregulated (adjusted p-value < 0.001 and $\log_2$(fold-change) < -2) and upregulated
905 (adjusted p-value < 0.001 and $\log_2$(fold-change) > 2) transposons are shown in cyan and magenta,
906 respectively. (C) Normalized number of reads for *Burdock* piRNAs from small RNA-seq.
907 Mean ± SD (n = 3.) P-value < 0.001 (Student's t-test, unpaired, two-tailed) is indicated by ***. (D)
908 The *Burdock* sensor harbors a *nanos* promoter, a nuclear localization signal (NLS) appended to
909 GFP and β-gal coding sequences, and a target sequence for *Burdock* piRNAs in the 3'UTR.
910 Confocal images of ovaries from control (y^{RNAi}) and *sakura*^{RNAi} flies harboring the Burdock sensor,
911 where RNAi knockdown was specifically driven in the female germline with *UAS-Dcr2* and *NGT-*

912 *Gal4*. GFP (green), β-gal (red), and DAPI (blue). Scale bars: 50 μm. Three out of 3 tested control
913 samples were negative for both GFP and β-gal, while 9 out of 9 tested *sakura*^{RNAi} samples were
914 positive for both markers.

915

916 **Fig 5. *sakura* is important for oogenesis in later-stage egg chambers**

917 (A) Stereomicroscope images of dissected whole ovaries. Scale bar: 500 μm. (B) Western blot of
918 dissected Ovary lysates. *sakura*$^{RNAi\ \#1}$ and *sakura*$^{RNAi\ \#2}$ are two independent RNAi lines. (C)
919 Number of eggs laid by *sakura* RNAi knockdown driven by *UAS-Dcr2* and *TOsk-Gal4*.
920 Mean ± SD (n = 5). P-value < 0.001 (Student's t-test, unpaired, two-tailed) is indicated by ***. (D)
921 Number of stage 14 oocytes produced by *sakura* RNAi knockdown flies driven by *UAS-Dcr2* and
922 *TOsk-Gal4*. P-value < 0.001 (Student's t-test, unpaired, two-tailed) is indicated by ***. (E)
923 Confocal images of the ovaries from *sakura* RNAi knockdown flies driven by *UAS-Dcr2* and
924 *TOsk-Gal4*, stained with anti-Orb and anti-Vasa antibodies. Orb (green), Vasa (red), and DAPI
925 (blue). Yellow arrows label the normal enrichment of Orb in the developing oocytes. Magenta
926 arrow labels mislocalized developing oocyte. White arrowheads label egg chambers with
927 cytoskeletal disorganization. Scale bars: 100 μm. In A-E, *y-RNAi* was used as a control.

928

929 **Fig 6. Germline clonal analysis of *sakura*^{null}**

930 (A) Percentage of germaria with marked GSC clones indicated by the absence of GFP at 4, 7, and
931 14 days after clone induction at the adult stage. Arrows indicate the percent decrease of marked
932 GSC clones compared to day 4. The genotype, actual percentage, and total number of germaria
933 examined are shown in the adjacent table. P-value < 0.01 (Chi-squared test) is indicated by **. (B)

934 Confocal images of Germ cell clones. *sakura*^{null} and control clones were marked by the absence of
935 GFP. GFP (green), Hts (red), and DAPI (blue). Scale bars: 10 μm. (C) Number of marked (GFP-
936 negative) GSC-like cells in germaria with marked GSCs of the indicated genotypes at 4, 7, and 14
937 days after clone induction. GSC-like cells containing round spectrosome were identified through
938 immunostaining with anti-Hts antibody. P-value < 0.05 and <0.001 (Student's t-test, unpaired, two-
939 tailed) is indicated by * and ***, respectively.

940

941 **Fig 7. Loss of *sakura* inhibits Dpp/BMP signaling**

942 (A) Confocal images of ovaries from control (y^{RNAi}) and *sakura*^{RNAi} flies harboring the *bam-GFP*
943 reporter, where RNAi knockdown was specifically driven in the female germline with *UAS-Dcr2*
944 and *NGT-Gal4*. Bam-GFP (green), Hts (red), and DAPI (blue). Germarium are outlined by dotted
945 line. Scale bars: 20 μm. (B, C) Confocal images of germaria with germline clones of *sakura*^{null}
946 stained with (B) anti-Bam antibody and (C) anti-pMad antibody. GFP (green), Bam or pMad (red),
947 and DAPI (blue). Scale bars: 10 μm. (D) Mean pMad intensity in the germline clones of the
948 indicated genotypes. Mean ± SD (n = 7). P-value < 0.001 (Student's t-test, unpaired, two-tailed) is
949 indicated by *** (E) Confocal images of germaria with germline clones of *sakura*^{null} stained with
950 anti-CycA antibody. GFP (green), CycA (red), and DAPI (blue). Scale bars: 10 μm. (F) Mean CycA
951 intensity in the germline clones of the indicated genotypes. Mean ± SD (n = 5 and 10 for *FRT82B*
952 and *FRT82B, sakura*^{null} respectively). P-value < 0.01 (Student's t-test, unpaired, two-tailed) is
953 indicated by **. In B, C, and E, clones were marked with the absence of GFP.

954

955 **Fig 8. Sakura interacts with Otu.**

956 (A) Co-immunoprecipitation using anti-GFP magnetic beads followed by Western blotting. Ovary
957 lysates expressing Sakura-EGFP in *sakura*$^{+/+}$ background and those from *w*^{1118} negative control
958 were tested. (B) Co-immunoprecipitation using beads bound with rabbit anti-Sakura followed by
959 Western blotting. Ovary lysates from *w*^{1118} flies were used. Rabbit IgG was used as control IP. (C)
960 Co-immunoprecipitation using beads bound with anti-FLAG antibody followed by Western
961 blotting. S2 cell lysates expressing 3xFLAG-Otu and Sakura-mCherry-3xHA or mCherry-3xHA
962 (negative control) were used.

963

964 **Fig 9. N-terminal regions of Sakura and Otu are important for interaction.**

965 (A) Predicted structure of the Sakura and Otu protein complex made by AlphaFold. Full-length
966 Sakura and N-terminal Otu fragment (N1. 1-405aa) were used for prediction. (B) Full-length Otu
967 and Otu fragments tested in co-immunoprecipitation assays. The binding assay results from (D) is
968 summarized. (C) Full-length Sakura and Sakura fragments tested in co-immunoprecipitation
969 assays (N: N-terminal, M: middle, C: C-terminal). The binding assay results from (E) is
970 summarized. (D, E, F) Co-immunoprecipitation using anti-HA magnetic beads followed by
971 Western blotting. S2 cell lysates expressing HA-tagged mCherry were used as negative controls.

972

973 **Fig 10. Loss of *otu* phenocopies loss of *sakura***

974 (A) Confocal images of ovaries from *otu-EGFP* and *otu(ΔTudor)-EGFP* transgenic flies. Otu-
975 EGFP and Otu(ΔTudor)-EGFP (green), DAPI (blue). Yellow arrows show the enrichment of Otu-
976 EGFP and Otu(ΔTudor)-EGFP in developing oocytes. Scale bars: 20 μm. (B) Stereomicroscope
977 images of dissected whole ovaries from *w*^{RNAi} (control) and *otu*^{RNAi} flies where RNAi knockdown

was driven in the female germline with *nos-Gal4-VP16* or *TOsk-Gal4*. Scale bar: 500 μm. (C) Western blot of dissected ovary lysates. (D) Number of eggs laid by *TOsk-Gal4* > w^{RNAi} and *TOsk-Gal4* > otu^{RNAi} flies. Mean ± SD (n = 5). P-value < 0.001 (Student's t-test, unpaired, two-tailed) are indicated by ***. (E) Violin plots of the number of stage 14 oocytes produced in *TOsk-Gal4* > w^{RNAi} and *TOsk-Gal4* > otu^{RNAi} flies. n = 30. P-value < 0.001 (Student's t-test, unpa©red, two-tailed) is indicated by ***.

Fig 11. Loss of *otu* results in low levels of pMad and derepression of *bam* in the germaria

(A) Confocal images of the ovaries from control (w^{RNAi}) and otu^{RNAi} flies harboring the *bam-GFP* reporter, where RNAi knockdown was driven in the female germline with *nos-Gal4-VP16*. Bam-GFP (green), Hts (red), and DAPI (blue). Scale bars: 20 μm. (B) Confocal images of germaria from control ($otu^{14/+}$) and $otu^{14/14}$ mutant flies stained with anti-pMad (green) and anti-Hts (red) antibodies. Scale bars: 10 μm. (C) Confocal images of the ovaries from *nos-Gal4-VP16* > w^{RNAi} and *nos-Gal4-VP16* > otu^{RNAi} flies stained with anti-cleaved Caspase 3 antibody. Cleaved Caspase-3 (red) and DAPI (blue). Scale bars: 20 μm. (D) Confocal images of the ovaries from w^{RNAi} and otu^{RNAi} flies carrying the Burdock sensor, with RNAi driven in the female germline using *UAS-Dcr2*, *NGT-Gal4* and *nos-Gal4-VP16*. GFP (green), β-gal (red), and DAPI (blue). Scale bars: 50 μm. Three out of 3 tested control samples were negative for both GFP and β-gal, while 14 out of 14 tested otu^{RNAi} samples were positive for positive for GFP and β-gal.

Fig 12. Otu enrichment to the posterior within egg chambers is lost in *sakura*^{null}

999 Confocal images of egg chambers with germline clones of *sakura*^{null} expressing (A) Otu-EGFP or
1000 (B) Otu(ΔTudor)-EGFP. Fly genotypes used: *hs-flp*/*w*; *otu-EGFP*/+; *FRT82B*, *ubi-RFP*/*FRT82B*.
1001 *hs-flp*/*w*; *otu-EGFP*/+; *FRT82B*, *ubi-RFP*/*FRT82B*, *sakura*^{null}. *hs-flp*/*w*; *otu(ΔTudor)-EGFP*/+;
1002 *FRT82B*, *ubi-RFP*/*FRT82B*. *hs-flp*/*w*; *otu(ΔTudor)-EGFP* /+; *FRT82B*, *ubi-RFP*/*FRT82B*,
1003 *sakura*^{null}. RFP (red), Otu-EGFP or Otu(ΔTudor)-EGFP (green), and DAPI (blue). Scale bars: 20
1004 μm. Marked clones (RFP-negative) are outlined with white dotted lines. Yellow arrows indicate
1005 normal posterior enrichment of Otu-EGFP and Otu(ΔTudor)-EGFP signal; magenta arrows
1006 indicate the loss of this posterior enrichment in *sakura*^{null} clones.

1007

1008 **Fig S1. Schematic illustration of bam expression regulation.**

1009 Cap cells secrete diffusible Decapentaplegic (Dpp), which is received by its receptor, a heterodimer
1010 of Thick vein (Tkv) and Punt (Put), in GSCs. The activated Dpp signaling eventually
1011 phosphorylates Mother-against-dpp (Mad). The phosphorylated Mad (pMad) represses the
1012 transcription of *bag-of-marbles* (*bam*). The repression of *bam* in GSCs is crucial for maintaining
1013 their stemness. Cystoblasts do not receive Dpp, and Bam expression is crucial for promoting
1014 cystoblast differentiation from GSCs.

1015

1016 **Fig S2. *sakura* mRNA expression pattern.**

1017 Data obtained from http://flybase.org/reports/FBgn0040602.htm.

1018

1019 **Fig S3. Male fertility assay.**

1020 The numbers of the progeny flies obtained from crosses between test males and wild-type
1021 (OregonR) virgin females are shown. Mean ± SD (n = 5).

1022

1023 **Fig S4. *sakura*^{null} ovaries are tumorous**

1024 Violin plots of GSC-like cell numbers in germaria of indicated genotypes of 2-5 days old flies.
1025 Mean ± SD and the biological replicate number n are also shown. P-value < 0.001 (Student's t-
1026 test, unpaired, two-tailed) is indicated by ***.

1027

1028 **Fig S5. The ratio of germless ovarioles increases over time in *sakura*^{null} ovaries**

1029 (A) Ratio (%) of normal, germless, and tumorous ovarioles of the indicated genotypes at 0-1 days,
1030 7 days, and 14 days post-eclosion. (B) Quantification of GSC-like cell numbers in ovarioles of the
1031 indicated genotypes of at 0-1 days, 7 days, and 14 days post-eclosion. Germless ovarioles were
1032 excluded from this analysis.

1033

1034 **Fig S6. Sex-specific alternative splicing of *sxl* is dysregulated in *sakura*^{null} ovaries**

1035 Sex-specific alternative splicing of *sxl* was analyzed by RT-CPR followed by agarose gel
1036 electrophoresis and SYBR Safe staining. Ovaries from controls and *sakura-EGFP* rescue flies
1037 showed the expected female-specific *sxl* isoform, while testes from control flies exhibited the
1038 male-specific isoform. *sakura*^{null} ovaries showed increased expression of the male-specific isoform
1039 and reduced levels of female-specific isoform.

1040

1041 **Fig S7. *sakura* is important for oogenesis in later-stage egg chambers**

1042 Confocal images of ovaries from *sakura* RNAi knockdown flies (*UAS-Dcr2*, *TOsk-Gal4 > sakura*
1043 ^{RNAi}) stained with phalloidin (F-Actin) and anti-Orb antibodies. F-Actin (red), Orb (green), and
1044 DAPI (blue). Yellow arrows indicate normal Orb enrichment at the posterior of developing
1045 oocytes. White arrowheads indicate egg chambers exhibiting cytoskeletal disorganization. Scale
1046 bars: 50 μm.

1047

1048 **Fig S8. *sakura*^{null} clone germline cells intrinsically cause tumorous phenotype**

1049 Number of GFP-positive GSC-like cells in germaria with marked (GFP-negative) GSCs of the
1050 indicated genotypes at 4, 7, and 14 days after clone induction. GSC-like cells containing round
1051 spectrosome were identified through immunostaining with anti-Hts antibody.

1052

1053 **Fig S9. Bam is not misexpressed in TOsk-Gal4 > *sakura*^{RNAi} egg chambers.**

1054 Confocal images of ovaries from *sakura* RNAi knockdown flies driven by *UAS-Dcr2* and *TOsk-*
1055 *Gal4*, stained with anti-Bam and anti-DE-Cadherin (DE-Cad) antibodies. *y-RNAi* was used as a
1056 control. Bam (green), DE-Cad (red), and DAPI (blue). Cyan arrowheads indicate high Bam
1057 expression in 8-cell cysts within the germarium. White arrowheads indicate egg chambers with
1058 cytoskeletal disorganization. Scale bars: 50 μm.

1059

1060 **Fig S10. Ratio of germless and tumorous phenotypes from double RNAi knockdown of**
1061 ***sakura* with *bam*, *cycA*, or *otu***

1062 (A) Ratio (%) of normal, germless, and tumorous ovarioles in double RNAi knockdown of *sakura*
1063 with *bam, cycA,* or *otu. UAS-Dcr2* and *NGT-Gal4* was used to drive RNAi knockdown in the
1064 germline. n is the total number of ovarioles examined for the indicated genotypes of 2-5 day-old
1065 flies. (B) Quantification of GSC-like cell number in germaria of indicated genotypes of 2-5 day-
1066 old flies. Germless ovarioles were excluded from this analysis.

1067

1068 **Fig S11. *nos-Gal4-VP16 > UASp-Mad-GFP* did not rescue the *sakura*^{null} phenotyopes**

1069 (A) Ratio (%) of normal, germless, and tumorous ovarioles in the indicated genotypes of 2-5 day-
1070 old flies. n denotes the total number of ovarioles examined for each genotype. (B) Quantification
1071 of GSC-like cell number in germaria of the indicated genotypes from 2-5 day-old flies. Germless
1072 ovarioles were excluded from this analysis.

1073

1074 **Fig S12. Ratio of germless and tumorous phenotypes in *sakura* RNAi knockdown and *NGT-***
1075 ***Gal4 > UASp-tkv.Q253D*.**

1076 (A) Ratio (%) of normal, germless, and tumorous ovarioles in the indicated genotypes of 2-5 day-
1077 old flies. RNAi knockdown and UASp-tkv.Q253D expression were driven with *UAS-Dcr2* and
1078 *NGT-Gal4*. n indicates the total number of ovarioles examined for each genotype. (B)
1079 Quantification of GSC-like cell number in germaria of the indicated genotypes from 2-5 day-old
1080 flies. Germless ovarioles were excluded from this analysis.

1081

1082 **Fig S13. anti-Otu Western blot of dissected ovary lysates.**

1083 (A) Western blot of dissected ovary lysates. (B) Western blot of dissected ovary lysates prepared
1084 from flies 2-5 hours and 3-7 days post eclosion and co-IP with anti-Sakura. The SDS-PAGE gel
1085 was run for a longer duration to better separate the 104 kDa and 98 kDa Otu isoforms. In 2-5 hour
1086 ovaries, the 104 kDa Otu isoform is more abundant, while in 3-7 day ovaries, the 98 kDa isoform
1087 predominates. Both Otu isoforms co-IPed with Sakura. The same 3-7 day ovary input and IP
1088 samples used for Fig 9B were used for anti-Otu and anti-Alpha-Tubulin Western. The anti-Sakura
1089 image is the same as shown in Fig 9B.

1090

1091 **Fig S14. Co-immunoprecipitations assay to test interaction between N-terminal fragments of**
1092 **Sakura and Otu in S2 cells**

1093 Co-immnuprocepitation assay using beads bound with anti-FLAG antibody followed by Western
1094 blotting. S2 cell lysates expressing mCherry-3xHA were used as controls. This is the reciprocal
1095 co-immunoprecipitation of Fig 9F.

1096

1097 **Fig S15. Depletion of Sakura does not deplete Otu and depletion of Otu does not deplete**
1098 **Sakura**

1099 (A) Western blot of dissected ovary lysates. The same samples used for Fig 5B were used for anti-
1100 Otu Western. The anti-Sakura and anti-Alpha tubulin images are the same as shown in Fig 5B. (B)
1101 The same samples used for Fig 10C were used for anti-Sakura Western. The anti-Otu and anti-
1102 Alpha tubulin images are the same as shown in Fig 10C.

1103

1104 **Fig S16. In vitro deubiquitination assay.**

1105 The mean fluorescence intensity of three replicates was plotted. Error bars (+/-) are standard
1106 deviations. Firefly Luciferase was used as a negative control.

1107

Identified protein name	Gene ID	Unique peptide counts					
		Sakura-EGFP samples			w1118 samples (negative control)		
		Replicate 1	Replicate 2	Replicate 3	Replicate 1	Replicate 2	Replicate 3
Ovarian tumor	CG12743	44	38	18	0	0	0
Uncharacterized protein Dmel_CG4679	CG4679	17	8	2	0	0	0
Uncharacterized protein Dmel_CG14997	CG14997	17	7	2	0	0	0
Mitochondrial ribosomal protein S22	CG12261	14	6	1	0	0	0
Tudor	CG9450	15	1	1	0	0	0
Mitochondrial ribosomal protein S5	CG40049	10	4	1	0	0	0
HECT and RLD domain containing protein 2	CG11734	4	9	1	0	0	0
Mitochondrial ribosomal protein S10	CG4247	5	3	1	0	0	0
Mitochondrial ribosomal protein S31	CG5904	3	1	1	0	0	0

Uncharacterized protein Dmel_CG1316	CG1316	2	1	1	0	0	0

1108

1109 **Table 1**. **Number of unique peptide counts detected by mass-spec**.

1110 Proteins with peptide signals present in all three biological replicates of the Sakura-EGFP
1111 samples without any signals in any of the three biological replicates of the negative control are
1112 shown.

1113

References

Bopp D, Horabin JI, Lersch RA, Cline TW, Schedl P. 1993. Expression of the Sex-lethal gene is controlled at multiple levels during Drosophila oogenesis. *Development* **118**: 797-812.

Casanueva MO, Ferguson EL. 2004. Germline stem cell number in the Drosophila ovary is regulated by redundant mechanisms that control Dpp signaling. *Development* **131**: 1881-1890.

Chau J, Kulnane LS, Salz HK. 2012. Sex-lethal enables germline stem cell differentiation by down-regulating Nanos protein levels during Drosophila oogenesis. *Proceedings of the National Academy of Sciences of the United States of America* **109**: 9465-9470.

Chen D, McKearin D. 2003a. Dpp signaling silences bam transcription directly to establish asymmetric divisions of germline stem cells. *Current biology : CB* **13**: 1786-1791.

Chen D, McKearin DM. 2003b. A discrete transcriptional silencer in the bam gene determines asymmetric division of the Drosophila germline stem cell. *Development* **130**: 1159-1170.

Chen D, Wang Q, Huang H, Xia L, Jiang X, Kan L, Sun Q, Chen D. 2009. Effete-mediated degradation of Cyclin A is essential for the maintenance of germline stem cells in Drosophila. *Development* **136**: 4133-4142.

Chu HP, Liao Y, Novak JS, Hu Z, Merkin JJ, Shymkiv Y, Braeckman BP, Dorovkov MV, Nguyen A, Clifford PM et al. 2014. Germline quality control: eEF2K stands guard to eliminate defective oocytes. *Developmental cell* **28**: 561-572.

Cox DN, Chao A, Baker J, Chang L, Qiao D, Lin H. 1998. A novel class of evolutionarily conserved genes defined by piwi are essential for stem cell self-renewal. *Genes & development* **12**: 3715-3727.

de Cuevas M, Matunis EL. 2011. The stem cell niche: lessons from the Drosophila testis. *Development* **138**: 2861-2869.

de Cuevas M, Spradling AC. 1998. Morphogenesis of the Drosophila fusome and its implications for oocyte specification. *Development* **125**: 2781-2789.

Donertas D, Sienski G, Brennecke J. 2013. Drosophila Gtsf1 is an essential component of the Piwi-mediated transcriptional silencing complex. *Genes & development* **27**: 1693-1705.

Eliazer S, Shalaby NA, Buszczak M. 2011. Loss of lysine-specific demethylase 1 nonautonomously causes stem cell tumors in the Drosophila ovary. *Proceedings of the National Academy of Sciences of the United States of America* **108**: 7064-7069.

ElMaghraby MF, Tirian L, Senti KA, Meixner K, Brennecke J. 2022. A genetic toolkit for studying transposon control in the Drosophila melanogaster ovary. *Genetics* **220**.

Fukunaga R, Colpan C, Han BW, Zamore PD. 2014. Inorganic phosphate blocks binding of pre-miRNA to Dicer-2 via its PAZ domain. *The EMBO journal* **33**: 371-384.

Fukunaga R, Doudna JA. 2009. dsRNA with 5' overhangs contributes to endogenous and antiviral RNA silencing pathways in plants. *The EMBO journal* **28**: 545-555.

Fukunaga R, Han BW, Hung JH, Xu J, Weng Z, Zamore PD. 2012. Dicer partner proteins tune the length of mature miRNAs in flies and mammals. *Cell* **151**: 533-546.

Gans M, Audit C, Masson M. 1975. Isolation and Characterization of Sex-Linked Female-Sterile Mutants in Drosophila-Melanogaster. *Genetics* **81**: 683-704.

1157 Gateff E, Kurzik-Dumke U, Wismar J, Loffler T, Habtemichael N, Konrad L, Dreschers S, Kaiser
1158 S, Protin U. 1996. Drosophila differentiation genes instrumental in tumor suppression. *Int*
1159 *J Dev Biol* **40**: 149-156.
1160 Gilboa L, Forbes A, Tazuke SI, Fuller MT, Lehmann R. 2003. Germ line stem cell differentiation in
1161 Drosophila requires gap junctions and proceeds via an intermediate state. *Development*
1162 **130**: 6625-6634.
1163 Glenn LE, Searles LL. 2001. Distinct domains mediate the early and late functions of the
1164 Drosophila ovarian tumor proteins. *Mechanisms of development* **102**: 181-191.
1165 Gollin SM, King RC. 1981. Studies of Fs(1)1621, a Mutation Producing Ovarian-Tumors in
1166 Drosophila-Melanogaster. *Developmental Genetics* **2**: 203-218.
1167 Grmai L, Pozmanter C, Van Doren M. 2022. The Regulation of Germline Sex Determination in
1168 Drosophila by Sex lethal. *Sex Dev* **16**: 323-328.
1169 Handler D, Meixner K, Pizka M, Lauss K, Schmied C, Gruber FS, Brennecke J. 2013. The genetic
1170 makeup of the Drosophila piRNA pathway. *Molecular cell* **50**: 762-777.
1171 Hayashi Y, Yoshinari Y, Kobayashi S, Niwa R. 2020. The regulation of Drosophila ovarian stem
1172 cell niches by signaling crosstalk. *Curr Opin Insect Sci* **37**: 23-29.
1173 Hinnant TD, Merkle JA, Ables ET. 2020. Coordinating Proliferation, Polarity, and Cell Fate in the
1174 Drosophila Female Germline. *Front Cell Dev Biol* **8**: 19.
1175 Huang X, Fejes Toth K, Aravin AA. 2017. piRNA Biogenesis in Drosophila melanogaster. *Trends*
1176 *Genet* **33**: 882-894.
1177 Ji S, Li C, Hu L, Liu K, Mei J, Luo Y, Tao Y, Xia Z, Sun Q, Chen D. 2017. Bam-dependent
1178 deubiquitinase complex can disrupt germ-line stem cell maintenance by targeting cyclin
1179 A. *Proceedings of the National Academy of Sciences of the United States of America* **114**:
1180 6316-6321.
1181 Ji S, Luo Y, Cai Q, Cao Z, Zhao Y, Mei J, Li C, Xia P, Xie Z, Xia Z et al. 2019. LC Domain-Mediated
1182 Coalescence Is Essential for Otu Enzymatic Activity to Extend Drosophila Lifespan.
1183 *Molecular cell* **74**: 363-377 e365.
1184 Jin Z, Flynt AS, Lai EC. 2013. Drosophila piwi mutants exhibit germline stem cell tumors that are
1185 sustained by elevated Dpp signaling. *Current biology : CB* **23**: 1442-1448.
1186 Jumper J, Evans R, Pritzel A, Green T, Figurnov M, Ronneberger O, Tunyasuvunakool K, Bates
1187 R, Zidek A, Potapenko A et al. 2021. Highly accurate protein structure prediction with
1188 AlphaFold. *Nature* **596**: 583-589.
1189 Kahney EW, Snedeker JC, Chen X. 2019. Regulation of Drosophila germline stem cells. *Current*
1190 *opinion in cell biology* **60**: 27-35.
1191 Kai T, Spradling A. 2003. An empty Drosophila stem cell niche reactivates the proliferation of
1192 ectopic cells. *Proceedings of the National Academy of Sciences of the United States of*
1193 *America* **100**: 4633-4638.
1194 Kandasamy SK, Fukunaga R. 2016. Phosphate-binding pocket in Dicer-2 PAZ domain for high-
1195 fidelity siRNA production. *Proceedings of the National Academy of Sciences of the United*
1196 *States of America* **113**: 14031-14036.
1197 Kandasamy SK, Zhu L, Fukunaga R. 2017. The C-terminal dsRNA-binding domain of Drosophila
1198 Dicer-2 is crucial for efficient and high-fidelity production of siRNA and loading of siRNA
1199 to Argonaute2. *Rna* **23**: 1139-1153.
1200 Kang I, Choi Y, Jung S, Lim JY, Lee D, Gupta S, Moon W, Shin C. 2018. Identification of target
1201 genes regulated by the Drosophila histone methyltransferase Eggless reveals a role of
1202 Decapentaplegic in apoptotic signaling. *Scientific reports* **8**: 7123.
1203 King RC, Mohler D, Riley SF, Storto PD, Nicolazzo PS. 1986. Complementation between alleles
1204 at the ovarian tumor locus of Drosophila melanogaster. *Dev Genet* **7**: 1-20.
1205 King RC, Riley SF. 1982. Ovarian Pathologies Generated by Various Alleles of the Otu Locus in
1206 Drosophila-Melanogaster. *Developmental Genetics* **3**: 69-89.

1207 Kirilly D, Xie T. 2007. The Drosophila ovary: an active stem cell community. *Cell research* **17**: 15-
1208 25.
1209 Levin HL, Moran JV. 2011. Dynamic interactions between transposable elements and their hosts.
1210 *Nature Reviews Genetics* **12**: 615-627.
1211 Li Y, Minor NT, Park JK, McKearin DM, Maines JZ. 2009. Bam and Bgcn antagonize Nanos-
1212 dependent germ-line stem cell maintenance. *Proceedings of the National Academy of*
1213 *Sciences of the United States of America* **106**: 9304-9309.
1214 Li Y, Zhang Q, Carreira-Rosario A, Maines JZ, McKearin DM, Buszczak M. 2013. Mei-p26
1215 cooperates with Bam, Bgcn and Sxl to promote early germline development in the
1216 Drosophila ovary. *PloS one* **8**: e58301.
1217 Liao SE, Ai Y, Fukunaga R. 2018. An RNA-binding protein Blanks plays important roles in defining
1218 small RNA and mRNA profiles in Drosophila testes. *Heliyon* **4**: e00706.
1219 Liao SE, Kandasamy SK, Zhu L, Fukunaga R. 2019. DEAD-box RNA helicase Belle post-
1220 transcriptionally promotes gene expression in an ATPase activity-dependent manner. *Rna*.
1221 Lin H. 1997. The tao of stem cells in the germline. *Annu Rev Genet* **31**: 455-491.
1222 Lin H, Spradling AC. 1993. Germline stem cell division and egg chamber development in
1223 transplanted Drosophila germaria. *Developmental biology* **159**: 140-152.
1224 Losick VP, Morris LX, Fox DT, Spradling A. 2011. Drosophila stem cell niches: a decade of
1225 discovery suggests a unified view of stem cell regulation. *Developmental cell* **21**: 159-171.
1226 McKearin D, Ohlstein B. 1995. A role for the Drosophila bag-of-marbles protein in the
1227 differentiation of cystoblasts from germline stem cells. *Development* **121**: 2937-2947.
1228 McKearin DM, Spradling AC. 1990. bag-of-marbles: a Drosophila gene required to initiate both
1229 male and female gametogenesis. *Genes & development* **4**: 2242-2251.
1230 Moon S, Cassani M, Lin YA, Wang L, Dou K, Zhang ZZ. 2018. A Robust Transposon-Endogenizing
1231 Response from Germline Stem Cells. *Developmental cell* **47**: 660-671 e663.
1232 Ohlstein B, Lavoie CA, Vef O, Gateff E, McKearin DM. 2000. The Drosophila cystoblast
1233 differentiation factor, benign gonial cell neoplasm, is related to DExH-box proteins and
1234 interacts genetically with bag-of-marbles. *Genetics* **155**: 1809-1819.
1235 Ohlstein B, McKearin D. 1997. Ectopic expression of the Drosophila Bam protein eliminates
1236 oogenic germline stem cells. *Development* **124**: 3651-3662.
1237 Ohtani H, Iwasaki YW, Shibuya A, Siomi H, Siomi MC, Saito K. 2013. DmGTSF1 is necessary for
1238 Piwi-piRISC-mediated transcriptional transposon silencing in the Drosophila ovary. *Genes*
1239 *& development* **27**: 1656-1661.
1240 Ota R, Kobayashi S. 2020. Myc plays an important role in Drosophila P-M hybrid dysgenesis to
1241 eliminate germline cells with genetic damage. *Commun Biol* **3**: 185.
1242 Pauli D, Oliver B, Mahowald AP. 1993. The role of the ovarian tumor locus in Drosophila
1243 melanogaster germ line sex determination. *Development* **119**: 123-134.
1244 Pek JW, Lim AK, Kai T. 2009. Drosophila maelstrom ensures proper germline stem cell lineage
1245 differentiation by repressing microRNA-7. *Developmental cell* **17**: 417-424.
1246 Penalva LO, Sanchez L. 2003. RNA binding protein sex-lethal (Sxl) and control of Drosophila sex
1247 determination and dosage compensation. *Microbiology and molecular biology reviews :*
1248 *MMBR* **67**: 343-359, table of contents.
1249 Rodesch C, Pettus J, Nagoshi RN. 1997. The Drosophila ovarian tumor gene is required for the
1250 organization of actin filaments during multiple stages in oogenesis. *Developmental biology*
1251 **190**: 153-164.
1252 Rubin T, Huynh JR. 2015. Mosaic Analysis in the Drosophila melanogaster Ovary. *Methods in*
1253 *molecular biology* **1328**: 29-55.
1254 Salz HK, Erickson JW. 2010. Sex determination in Drosophila: The view from the top. *Fly* **4**: 60-
1255 70.

1256 Sass GL, Comer AR, Searles LL. 1995. The ovarian tumor protein isoforms of Drosophila
1257 melanogaster exhibit differences in function, expression, and localization. *Developmental*
1258 *biology* **167**: 201-212.
1259 Siomi MC, Sato K, Pezic D, Aravin AA. 2011. PIWI-interacting small RNAs: the vanguard of
1260 genome defence. *Nature reviews Molecular cell biology* **12**: 246-258.
1261 Smith PA, King RC. 1966. Studies on Fused a Mutant Gene Producing Ovarian Tumors in
1262 Drosophila Melanogaster. *Genetics* **54**: 363-&.
1263 Song X, Wong MD, Kawase E, Xi R, Ding BC, McCarthy JJ, Xie T. 2004. Bmp signals from niche
1264 cells directly repress transcription of a differentiation-promoting gene, bag of marbles, in
1265 germline stem cells in the Drosophila ovary. *Development* **131**: 1353-1364.
1266 Song X, Zhu CH, Doan C, Xie T. 2002. Germline stem cells anchored by adherens junctions in
1267 the Drosophila ovary niches. *Science* **296**: 1855-1857.
1268 Steinhauer WR, Kalfayan LJ. 1992a. A specific ovarian tumor protein isoform is required for
1269 efficient differentiation of germ cells in Drosophila oogenesis. *Genes & development* **6**:
1270 233-243.
1271 -. 1992b. A Specific Ovarian Tumor Protein Isoform Is Required for Efficient Differentiation of
1272 Germ-Cells in Drosophila Oogenesis. *Genes & development* **6**: 233-243.
1273 Storto PD, King RC. 1987. Fertile heteroallelic combinations of mutant alleles of the otu locus of
1274 Drosophila melanogaster. *Rouxs Arch Dev Biol* **196**: 210-221.
1275 -. 1988. Multiplicity of functions for the otu gene products during Drosophila oogenesis. *Dev Genet*
1276 **9**: 91-120.
1277 Van Buskirk C, Schupbach T. 2002. Half pint regulates alternative splice site selection in
1278 Drosophila. *Developmental cell* **2**: 343-353.
1279 Wang Z, Lin H. 2004. Nanos maintains germline stem cell self-renewal by preventing
1280 differentiation. *Science* **303**: 2016-2019.
1281 Xia L, Jia S, Huang S, Wang H, Zhu Y, Mu Y, Kan L, Zheng W, Wu D, Li X et al. 2010. The
1282 Fused/Smurf complex controls the fate of Drosophila germline stem cells by generating a
1283 gradient BMP response. *Cell* **143**: 978-990.
1284 Xie T, Spradling AC. 1998. decapentaplegic is essential for the maintenance and division of
1285 germline stem cells in the Drosophila ovary. *Cell* **94**: 251-260.
1286 Xu T, Rubin GM. 1993. Analysis of genetic mosaics in developing and adult Drosophila tissues.
1287 *Development* **117**: 1223-1237.
1288 Yamashiro H, Siomi MC. 2018. PIWI-Interacting RNA in Drosophila: Biogenesis, Transposon
1289 Regulation, and Beyond. *Chem Rev* **118**: 4404-4421.
1290 Yang F, Quan Z, Huang H, He M, Liu X, Cai T, Xi R. 2019. Ovaries absent links dLsd1 to HP1a
1291 for local H3K4 demethylation required for heterochromatic gene silencing. *eLife* **8**.
1292 Yang L, Chen D, Duan R, Xia L, Wang J, Qurashi A, Jin P, Chen D. 2007. Argonaute 1 regulates
1293 the fate of germline stem cells in Drosophila. *Development* **134**: 4265-4272.
1294 Yang Z, Zeng X, Zhao Y, Chen R. 2023. AlphaFold2 and its applications in the fields of biology
1295 and medicine. *Signal Transduct Target Ther* **8**: 115.
1296 Zhu L, Fukunaga R. 2021. RNA-binding protein Maca is crucial for gigantic male fertility factor
1297 gene expression, spermatogenesis, and male fertility, in Drosophila. *PLoS genetics* **17**:
1298 e1009655.
1299 Zhu L, Kandasamy SK, Fukunaga R. 2018a. Dicer partner protein tunes the length of miRNAs
1300 using base-mismatch in the pre-miRNA stem. *Nucleic acids research*.
1301 Zhu L, Kandasamy SK, Liao SE, Fukunaga R. 2018b. LOTUS domain protein MARF1 binds
1302 CCR4-NOT deadenylase complex to post-transcriptionally regulate gene expression in
1303 oocytes. *Nature communications* **9**: 4031.
1304 Zhu L, Liao SE, Ai Y, Fukunaga R. 2019a. RNA methyltransferase BCDIN3D is crucial for female
1305 fertility and miRNA and mRNA profiles in Drosophila ovaries. *PloS one* **14**: e0217603.

1306 Zhu L, Liao SE, Fukunaga R. 2019b. Drosophila Regnase-1 RNase is required for mRNA and
1307 miRNA profile remodelling during larva-to-adult metamorphosis. *RNA biology* **16**: 1386-
1308 1400.

1309

Figure 1. Azlan et al.

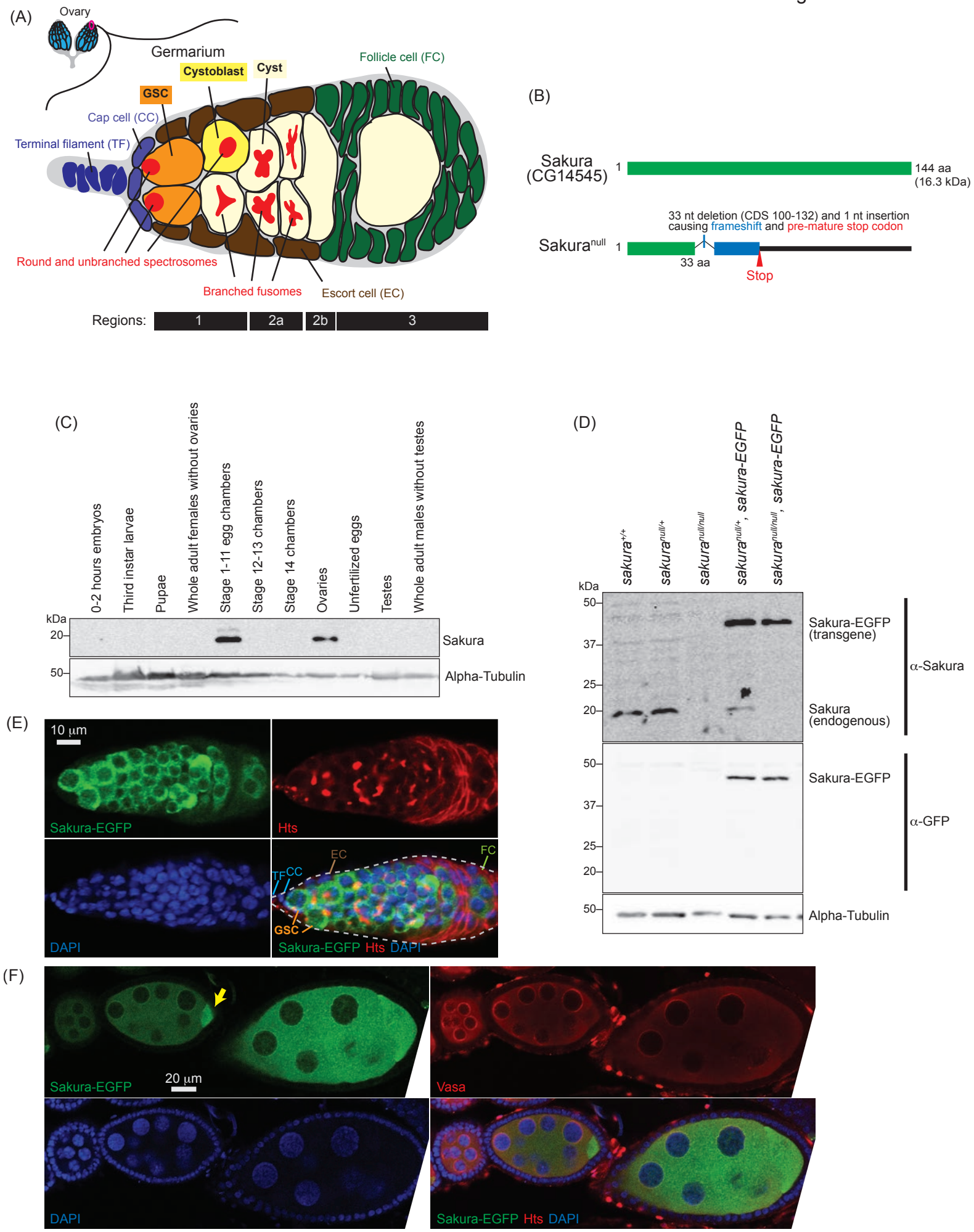

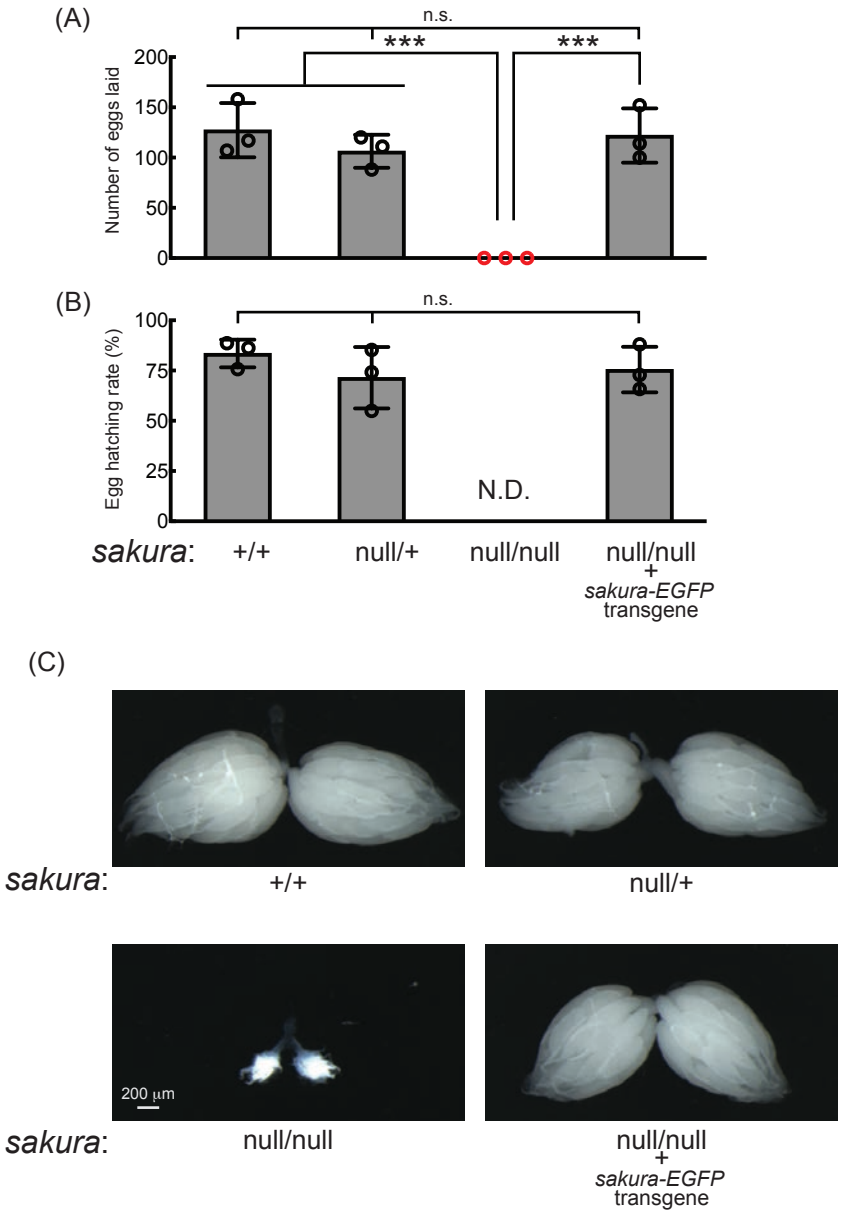
(A)
n.s.
***
***
Number of eggs laid
200
150
100
50
0
(B)
n.s.
Egg hatching rate (%)
100
75
50
25
0
N.D.
sakura: +/+
null/+
null/null
null/null + sakura-EGFP transgene
(C)
sakura: +/+
null/+
200 µm
sakura: null/null
null/null + sakura-EGFP transgene

Figure 3. Azlan et al.

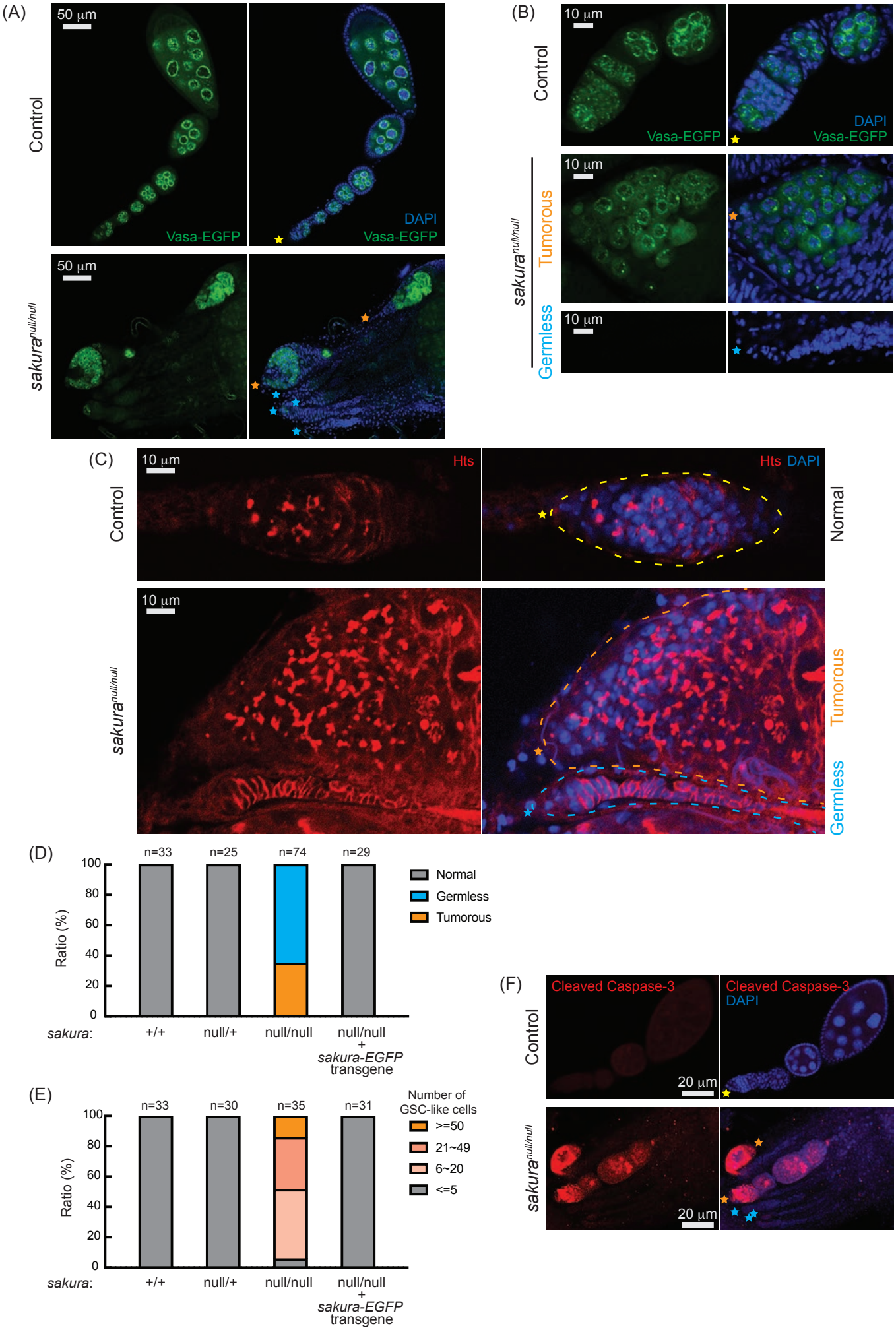

(A) piRNA expression

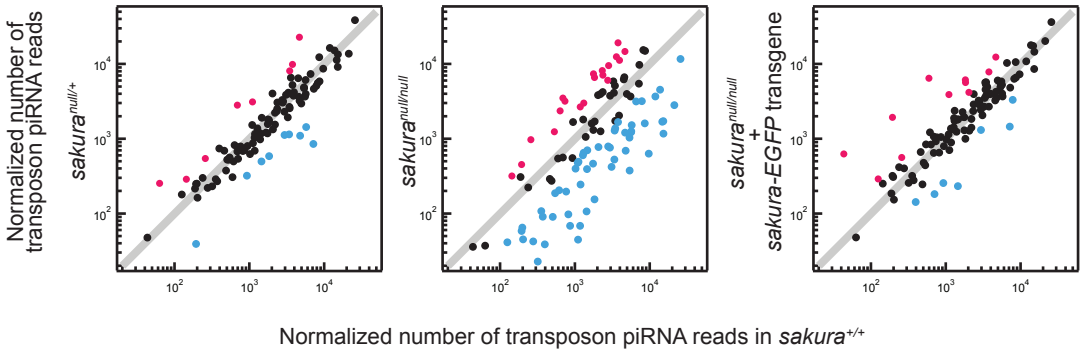

(B) Transposon RNA expression

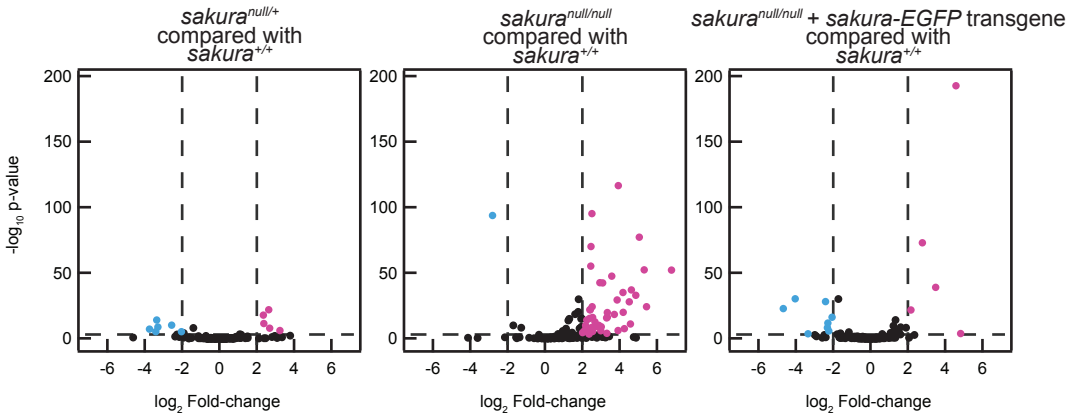

(C)

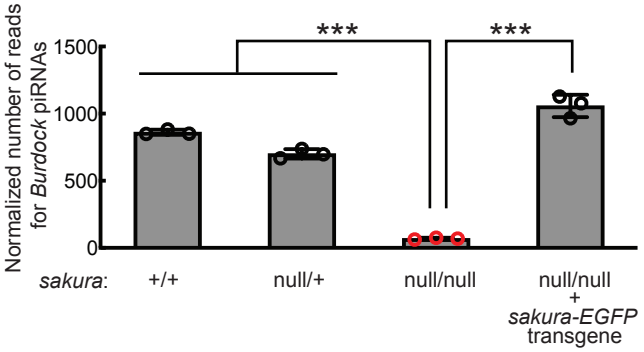

(D)

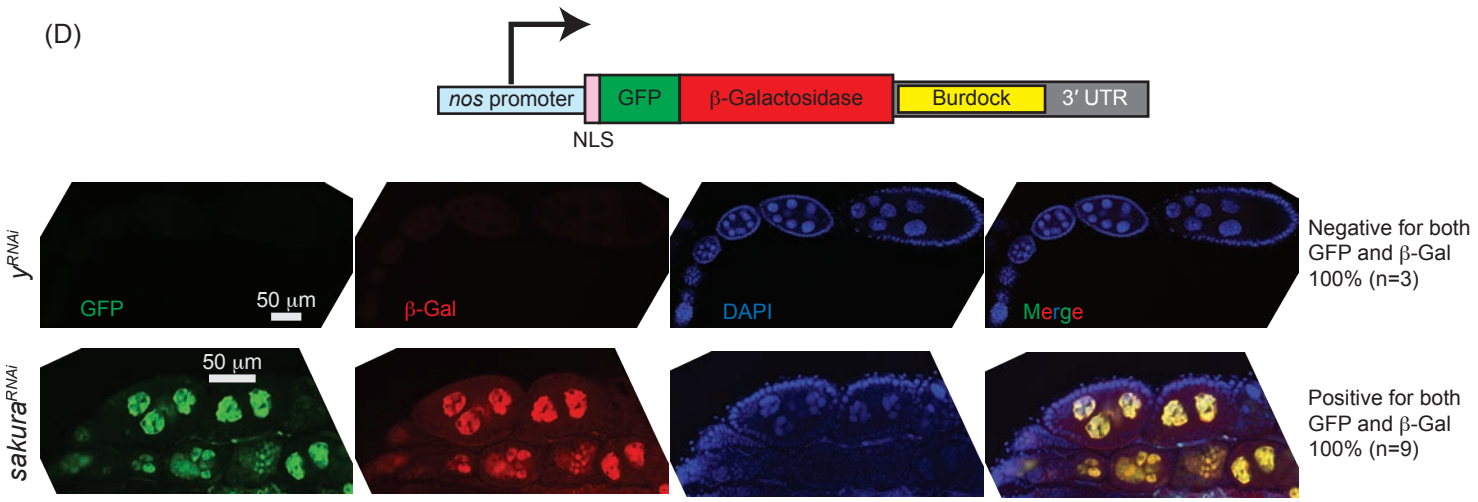

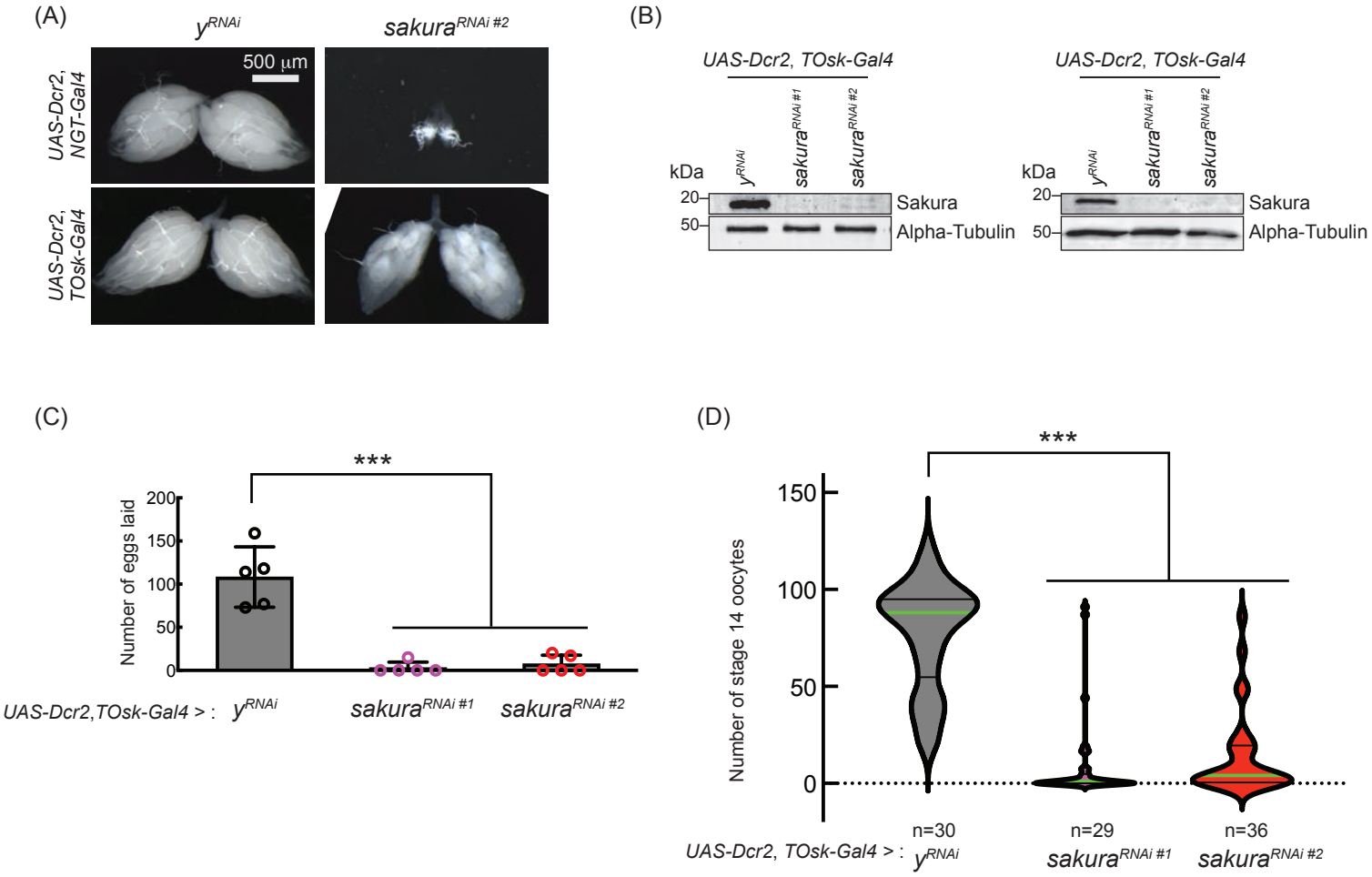
(A)
y RNAi
sakura RNAi #2
500 µm
UAS-Dcr2, NGT-Gal4
UAS-Dcr2, TOsk-Gal4
(B)
UAS-Dcr2, TOsk-Gal4
UAS-Dcr2, TOsk-Gal4
kDa
y RNAi
sakura RNAi #1
sakura RNAi #2
20
50
Sakura
Alpha-Tubulin
(C)
***
Number of eggs laid
200
150
100
50
0
UAS-Dcr2,TOsk-Gal4 > :
y RNAi
sakura RNAi #1
sakura RNAi #2
(D)
***
Number of stage 14 oocytes
150
100
50
0
n=30
n=29
n=36
UAS-Dcr2, TOsk-Gal4 > :
y RNAi
sakura RNAi #1
sakura RNAi #2

(E)

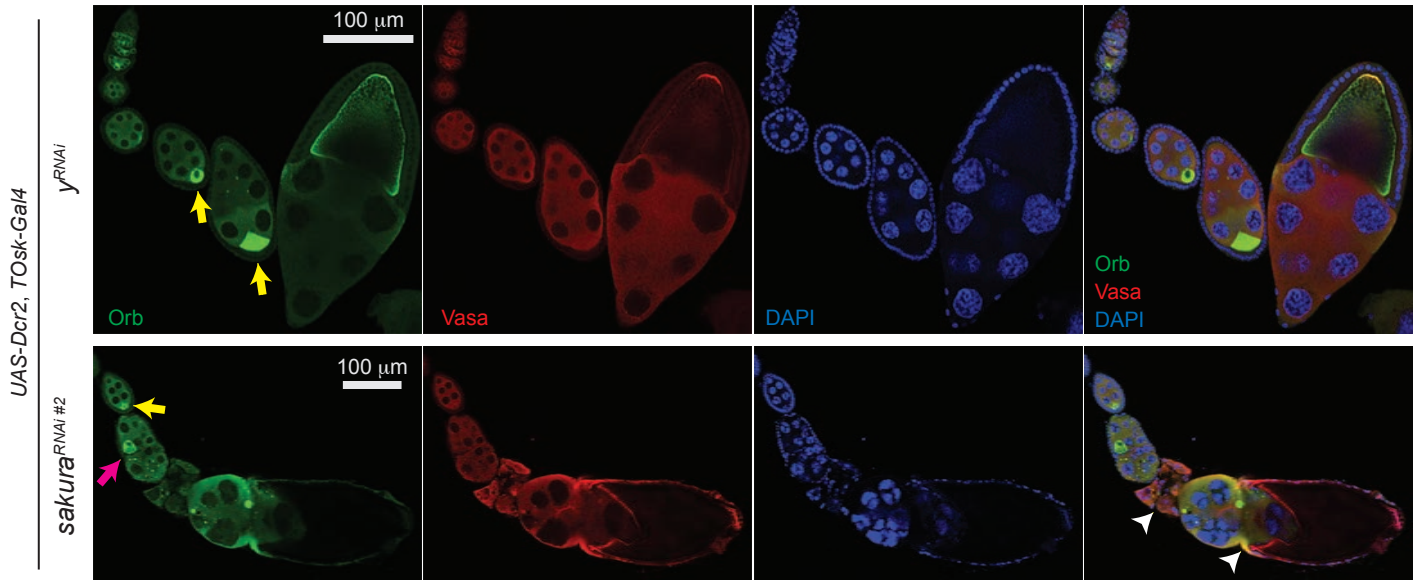
UAS-Dcr2, TOsk-Gal4
y RNAi
sakura RNAi #2
100 µm
Orb
Vasa
DAPI
Orb
Vasa
DAPI
100 µm

(A)

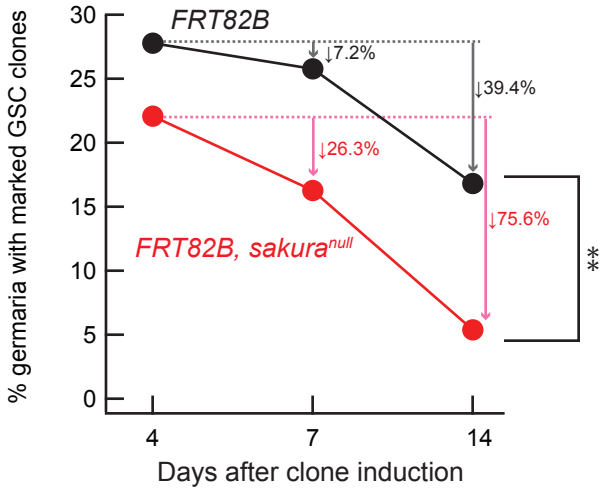

Genotype	Days after stopping heat shock	% marked GSCs	Relative % marked GSCs	Total number of germaria examined
hs-flp/w; +; FRT82B, ubi-GFP / FRT82B (control)	4	27.8	100	108
	7	25.8	92.8	97
	14	16.8	60.6	101
hs-flp/w; +; FRT82B, ubi-GFP / FRT82B, sakura^null	4	22.1	100	77
	7	16.3	73.7	86
	14	5.4	24.4	167

(B)

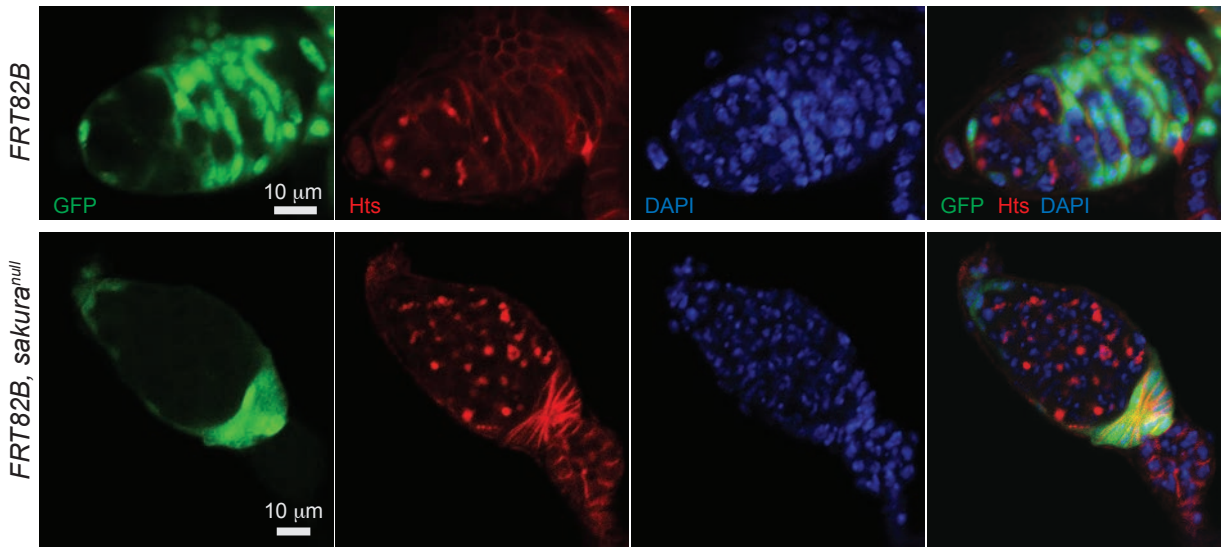

(C)

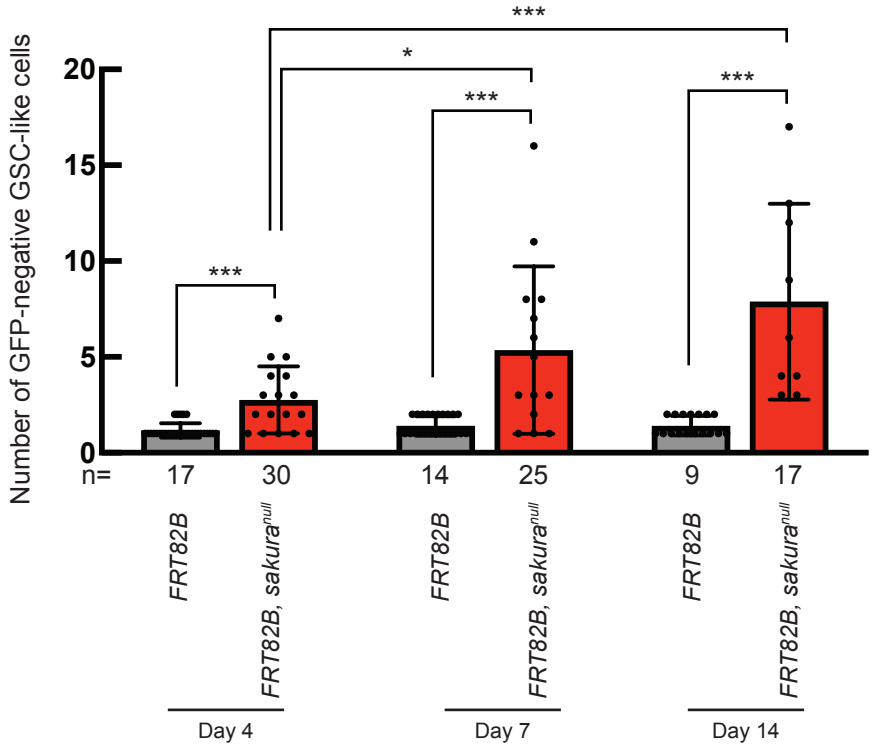

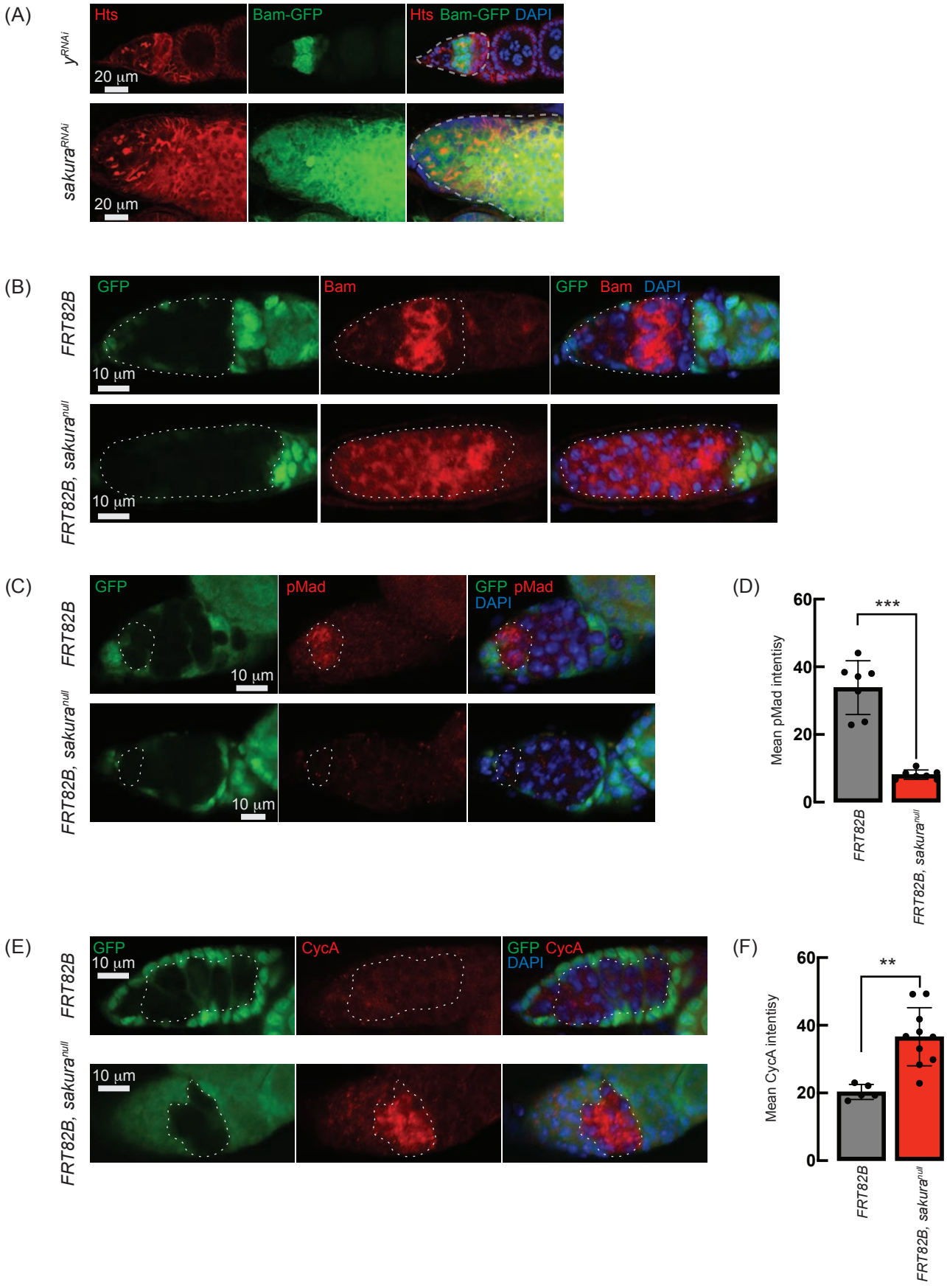
(A)
Hts
Bam-GFP
Hts Bam-GFP DAPI
y^RNAi
sakura^RNAi
20 µm
20 µm
(B)
GFP
Bam
GFP Bam DAPI
FRT82B
FRT82B, sakura^null
10 µm
10 µm
(C)
GFP
pMad
GFP pMad DAPI
FRT82B
FRT82B, sakura^null
10 µm
10 µm
(D)
Mean pMad intentisy
60
40
20
0
***
FRT82B
FRT82B, sakura^null
(E)
GFP
CycA
GFP CycA DAPI
FRT82B
FRT82B, sakura^null
10 µm
10 µm
(F)
Mean CycA intentisy
60
40
20
0
**
FRT82B
FRT82B, sakura^null

Figure 8. Azlan et al.

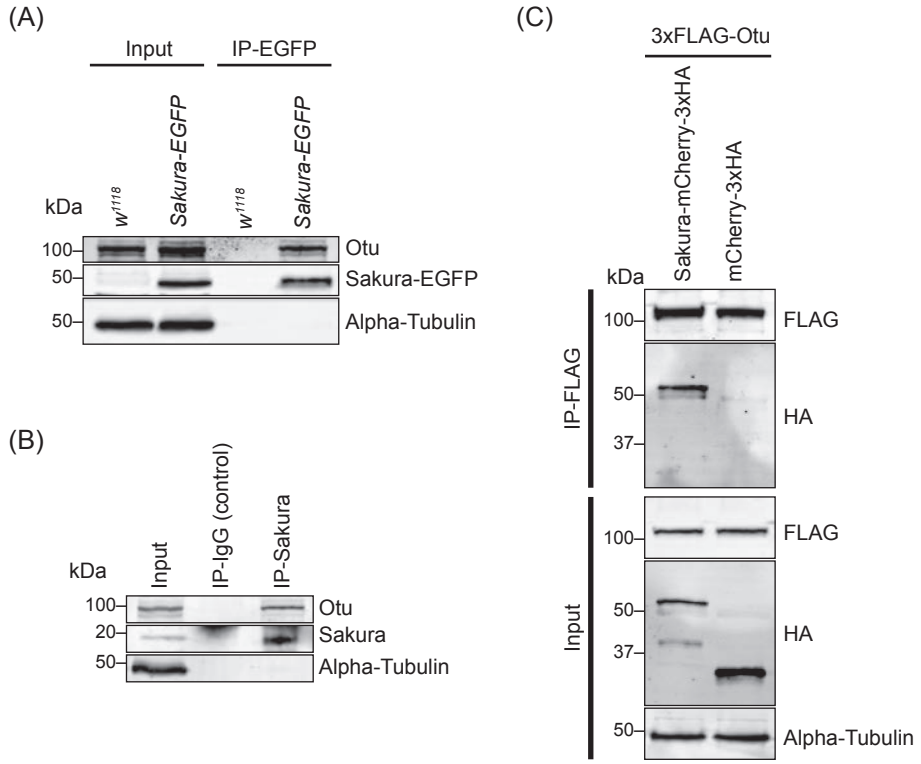

Figure 9. Azlan et al.

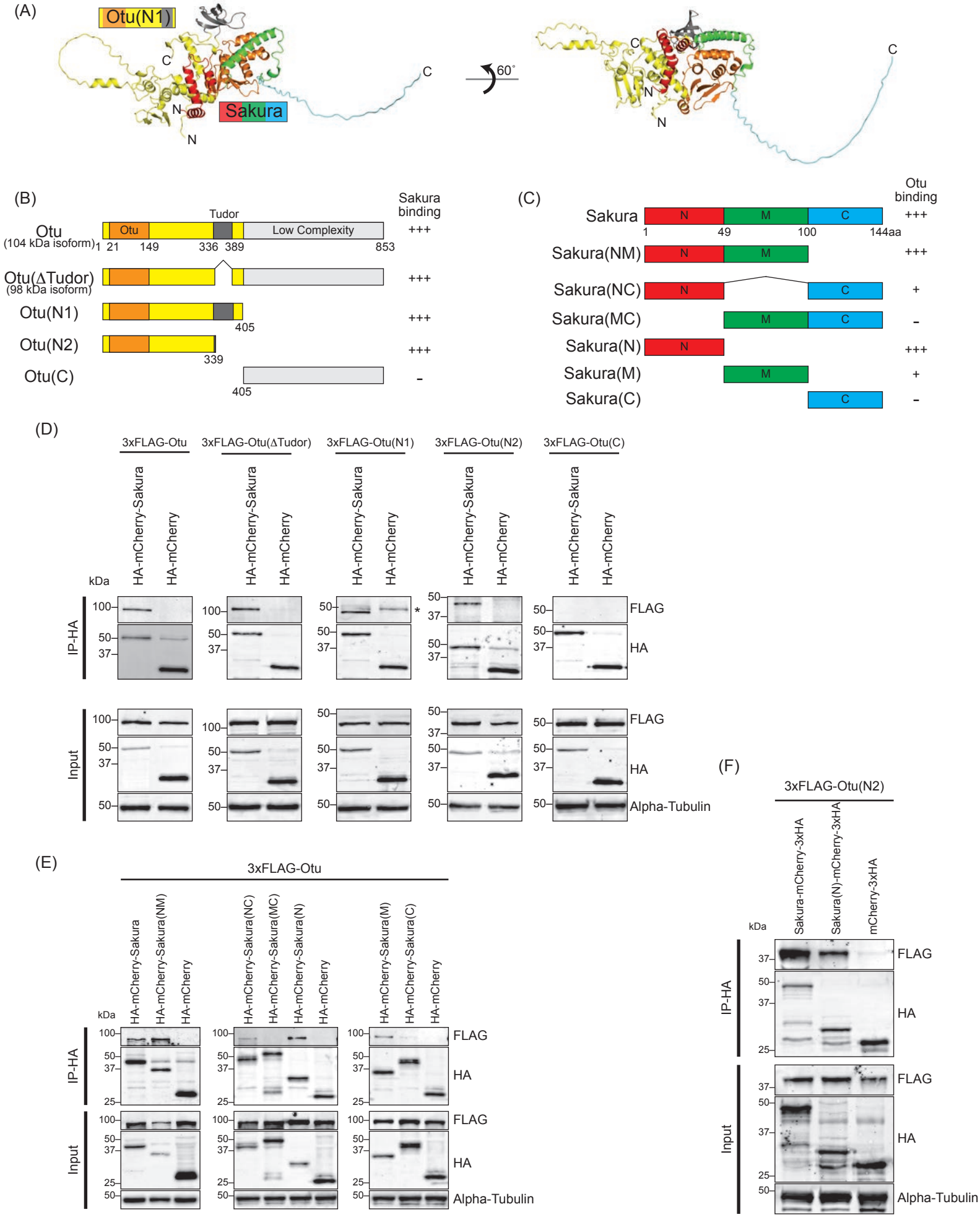

(A)

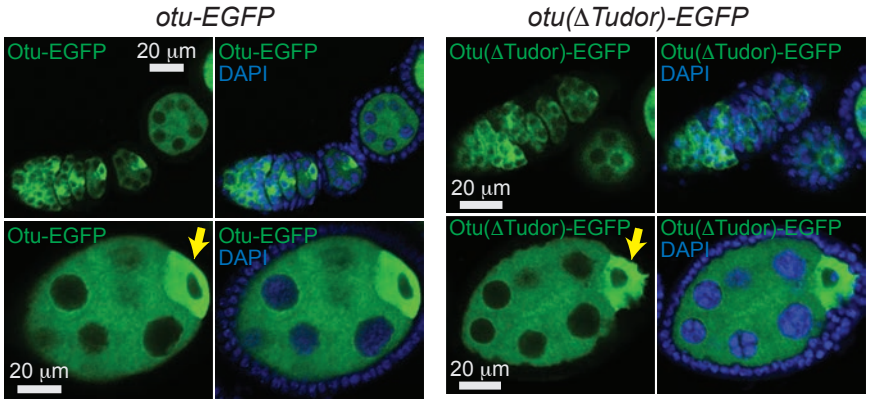
otu-EGFP
otu(ΔTudor)-EGFP
Otu-EGFP
20 μm
Otu-EGFP
DAPI
Otu(ΔTudor)-EGFP
Otu(ΔTudor)-EGFP
DAPI
20 μm
Otu-EGFP
Otu-EGFP
DAPI
20 μm
Otu(ΔTudor)-EGFP
Otu(ΔTudor)-EGFP
DAPI
20 μm

(B)

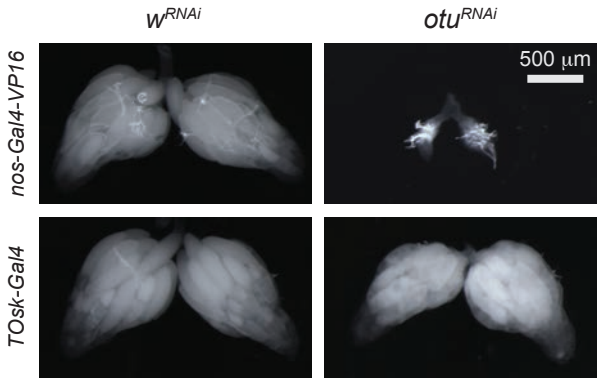
wRNAi
otuRNAi
500 μm
nos-Gal4-VP16
TOsk-Gal4

(C)

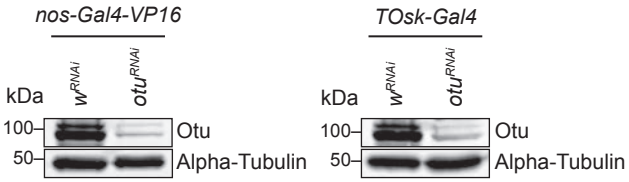
nos-Gal4-VP16
TOsk-Gal4
kDa
wRNAi
otuRNAi
100
50
Otu
Alpha-Tubulin

(D)

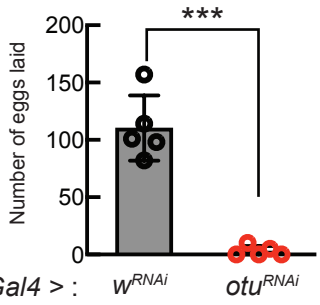
Number of eggs laid
200
150
100
50
0
***
TOsk-Gal4 > :
wRNAi
otuRNAi

(E)

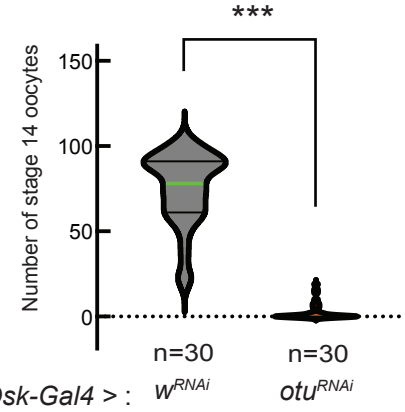
***
Number of stage 14 oocytes
150
100
50
0
n=30
n=30
TOsk-Gal4 > :
wRNAi
otuRNAi

Figure 11. Azlan et al.

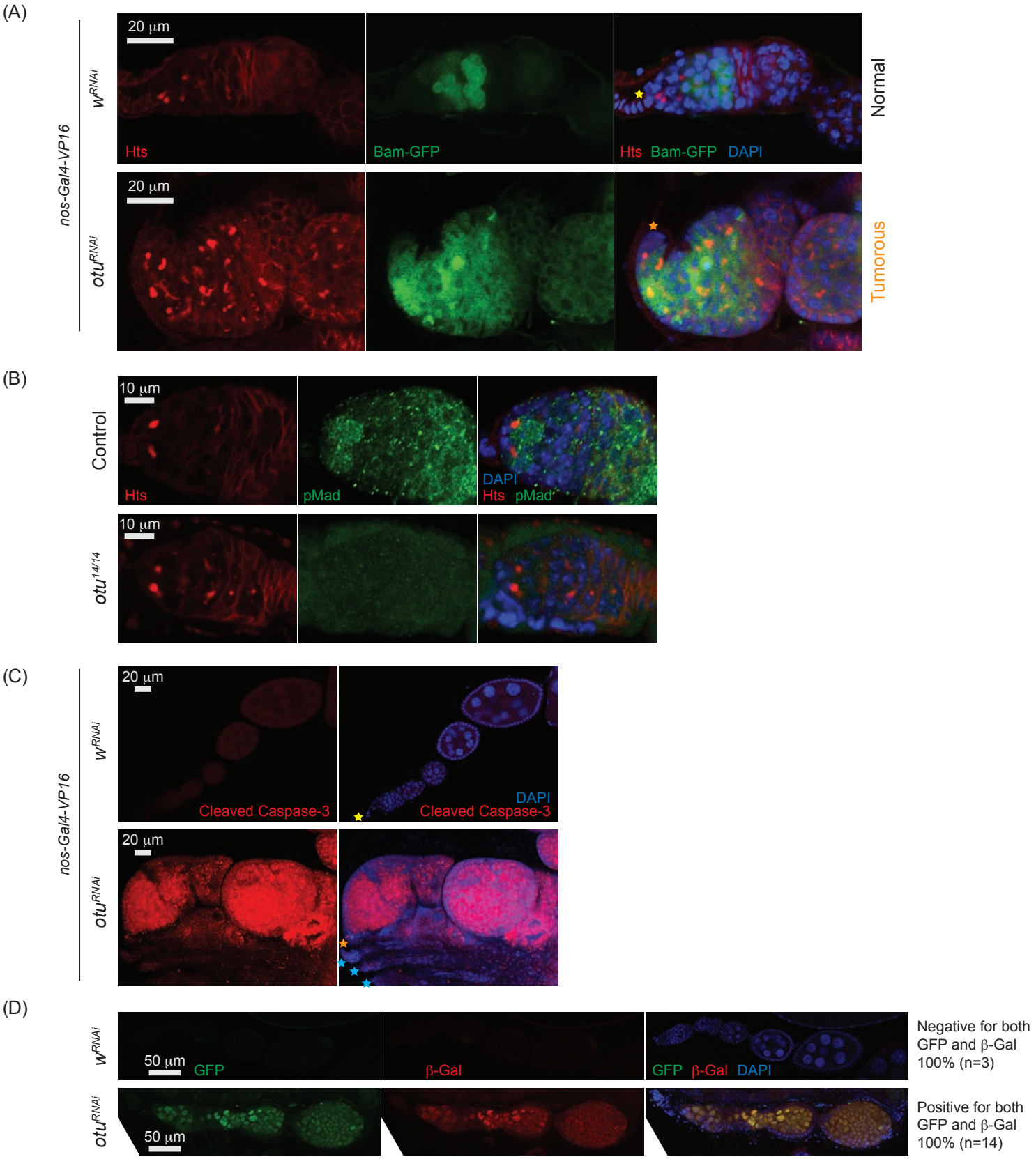

Figure 12. Azlan et al.

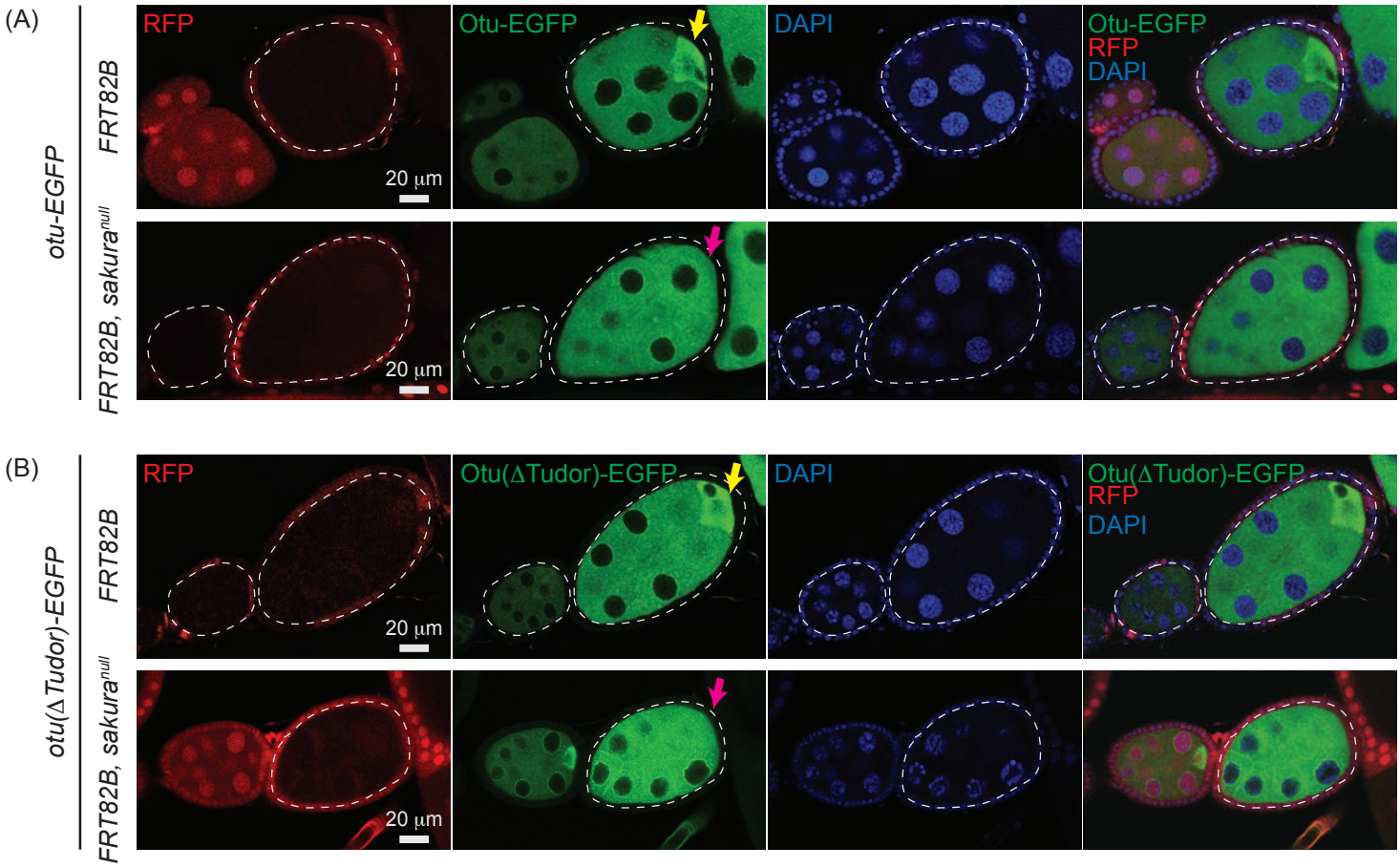

Figure S1. Azlan et al.

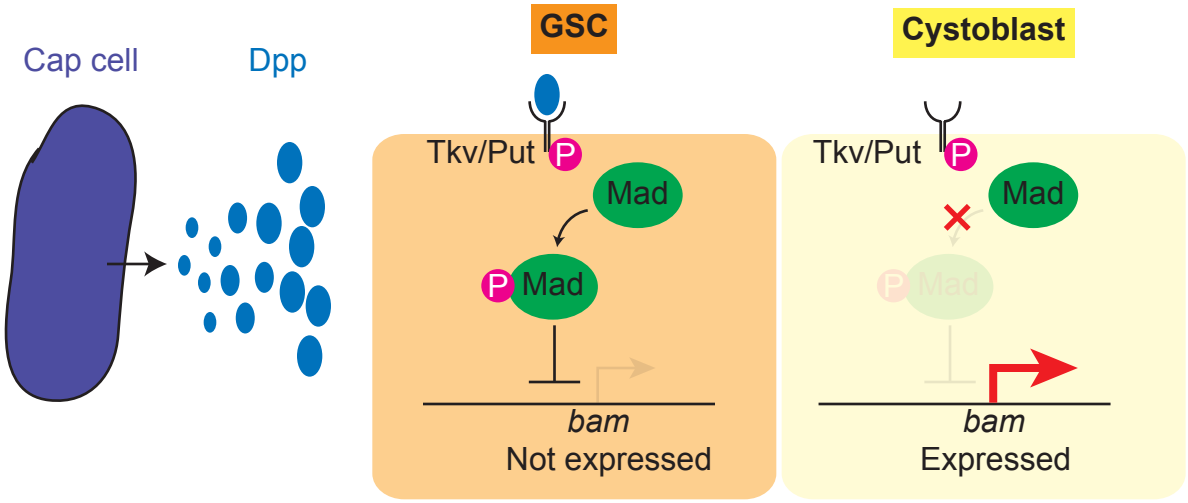

Figure S2. Azlan et al.

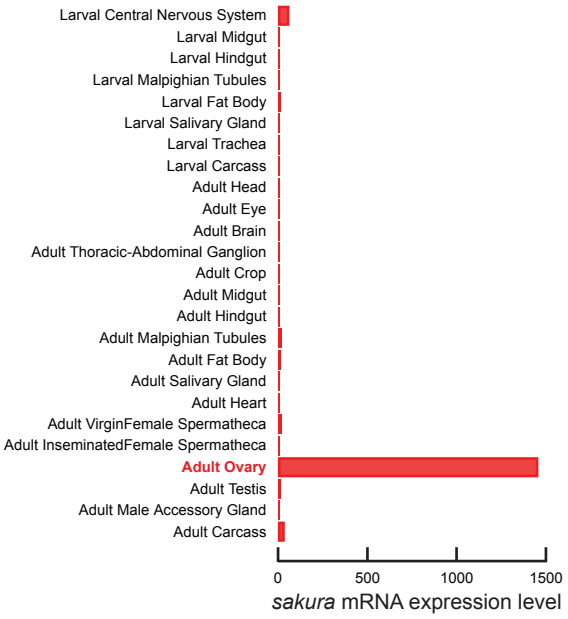

Figure S3. Azlan et al.

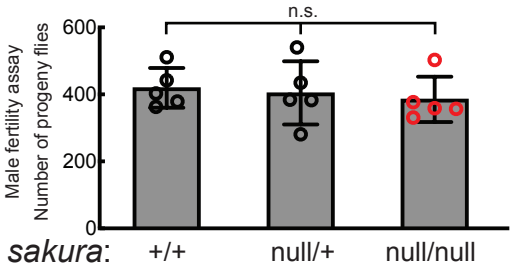

Figure S4. Azlan et al.

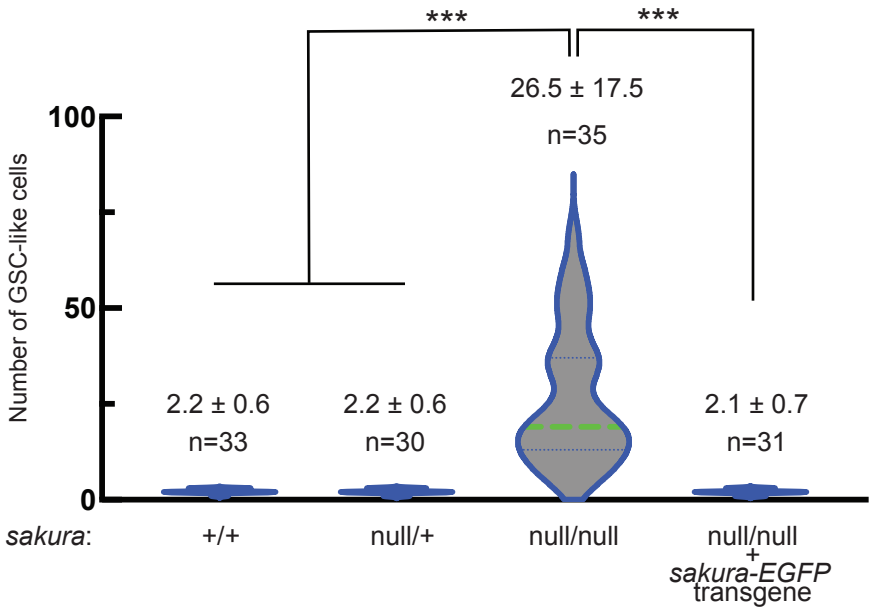

Figure S5. Azlan et al.

(A)

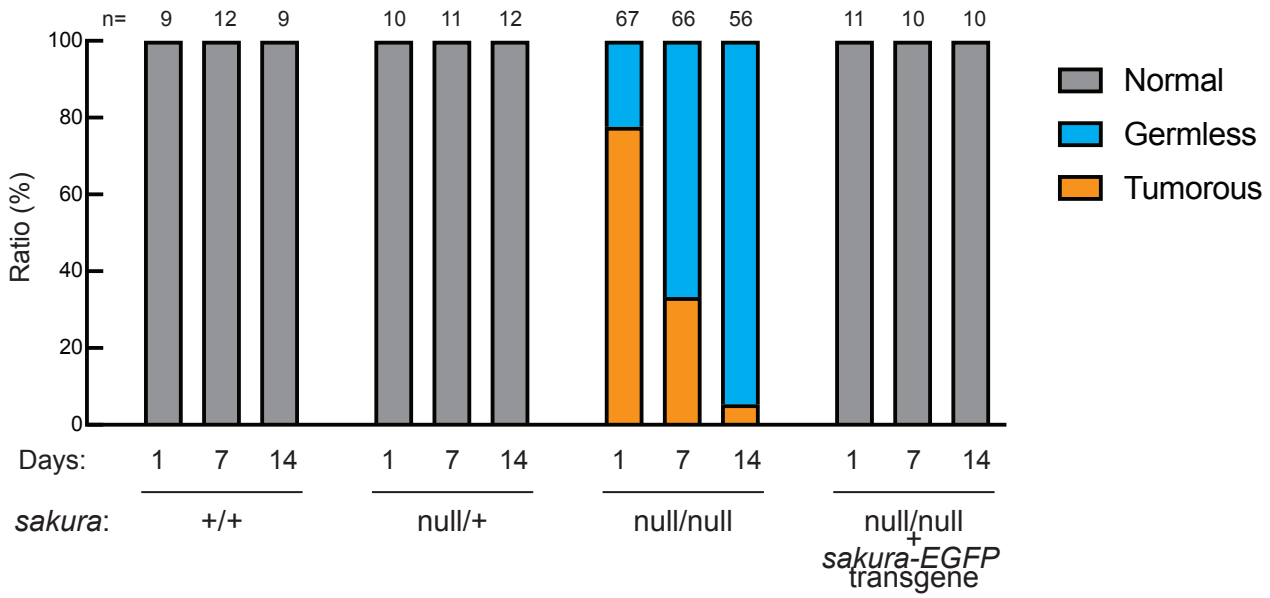

(B)

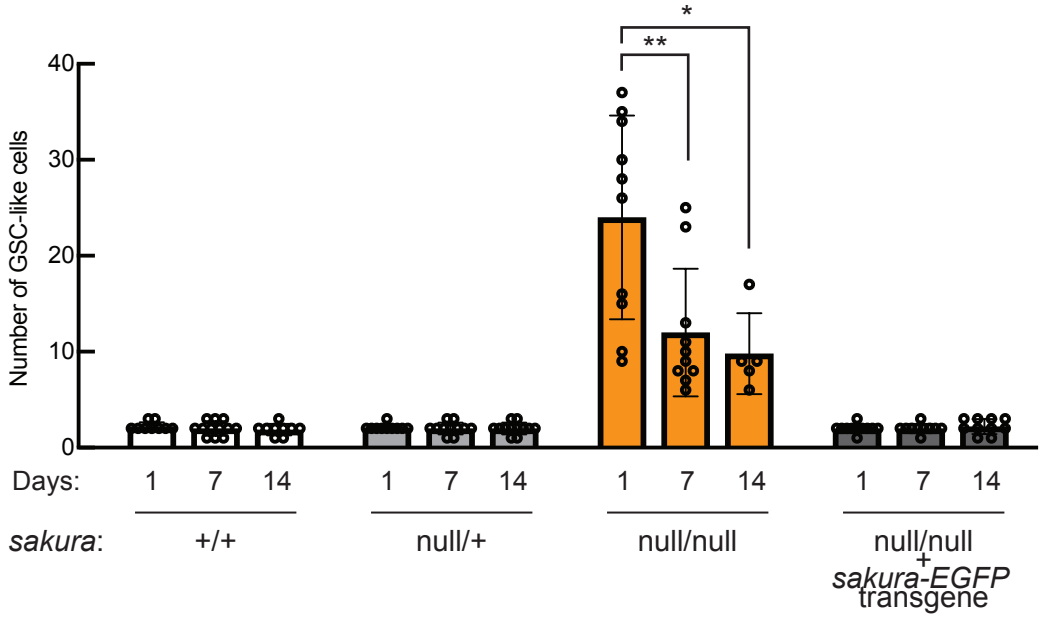

Figure S6. Azlan et al.

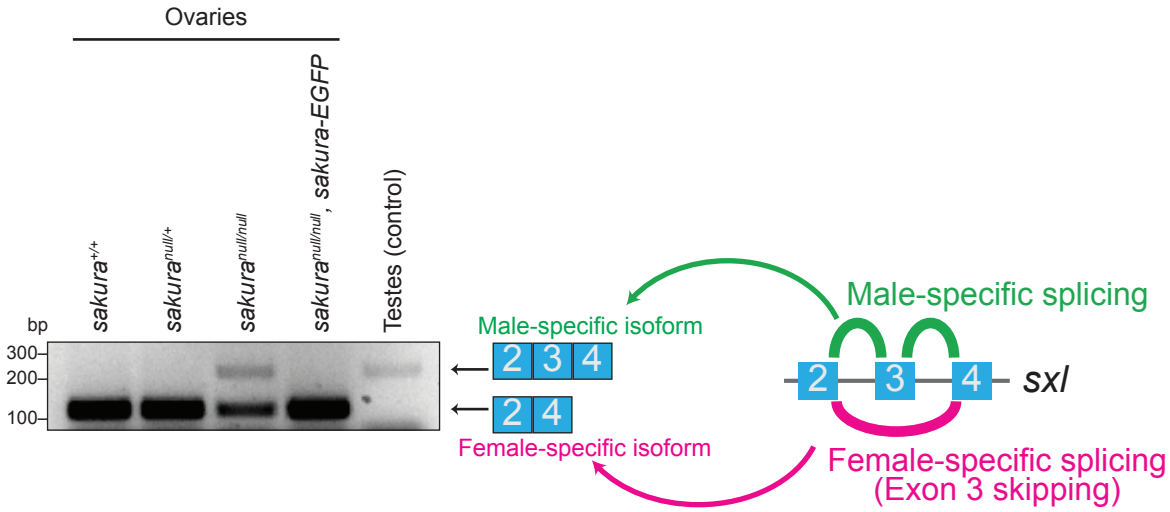

Figure S7. Azlan et al.

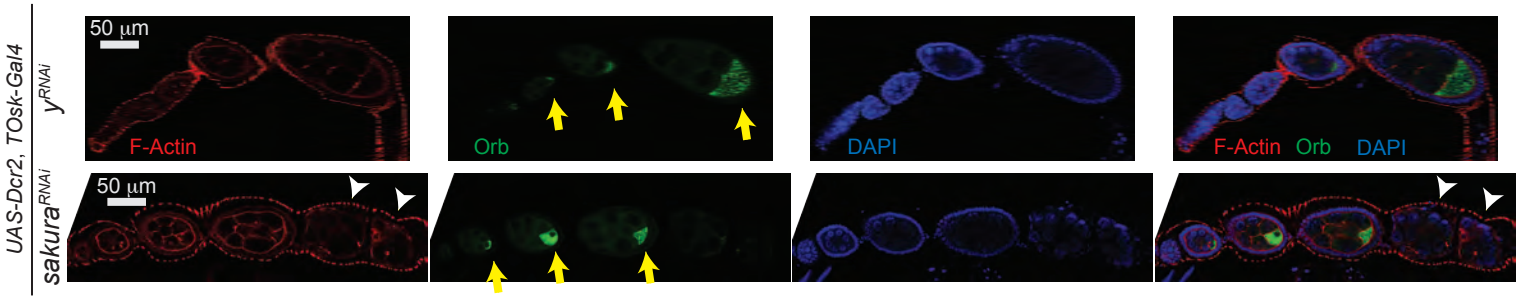

Figure S8. Azlan et al.

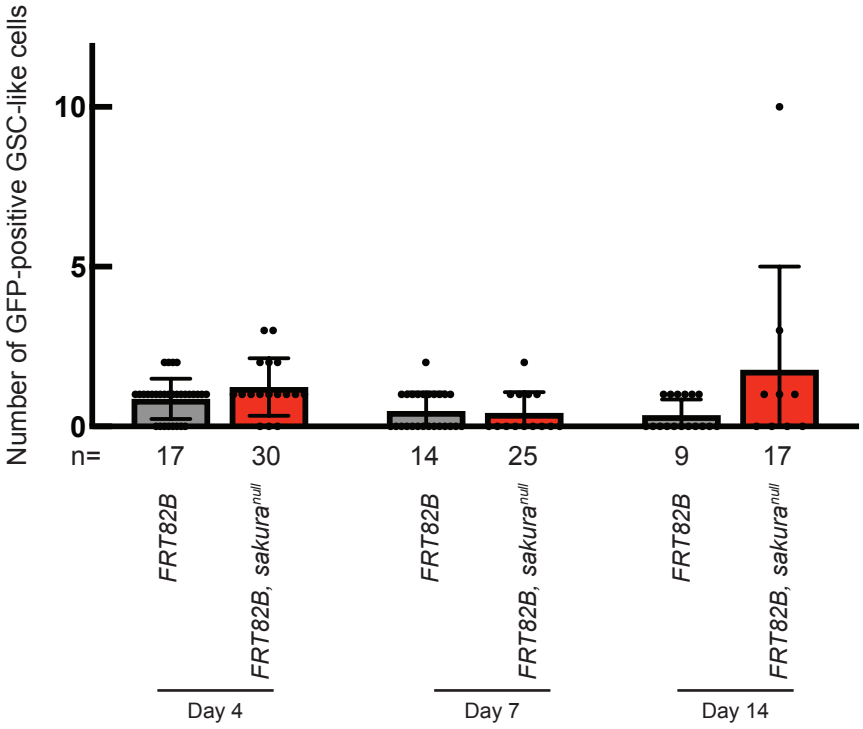

Figure S9. Azlan et al.

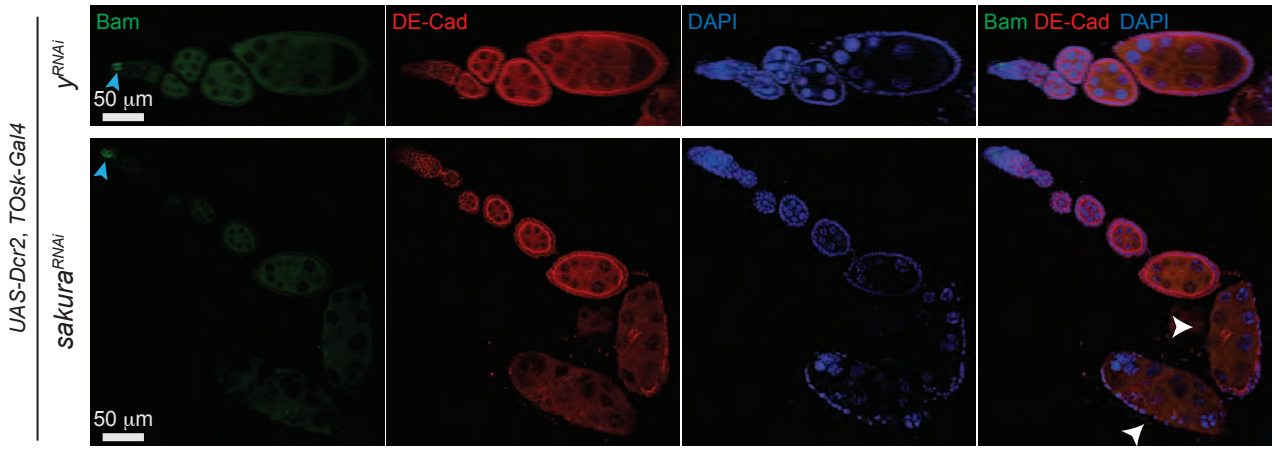

Figure S10. Azlan et al.

(A)

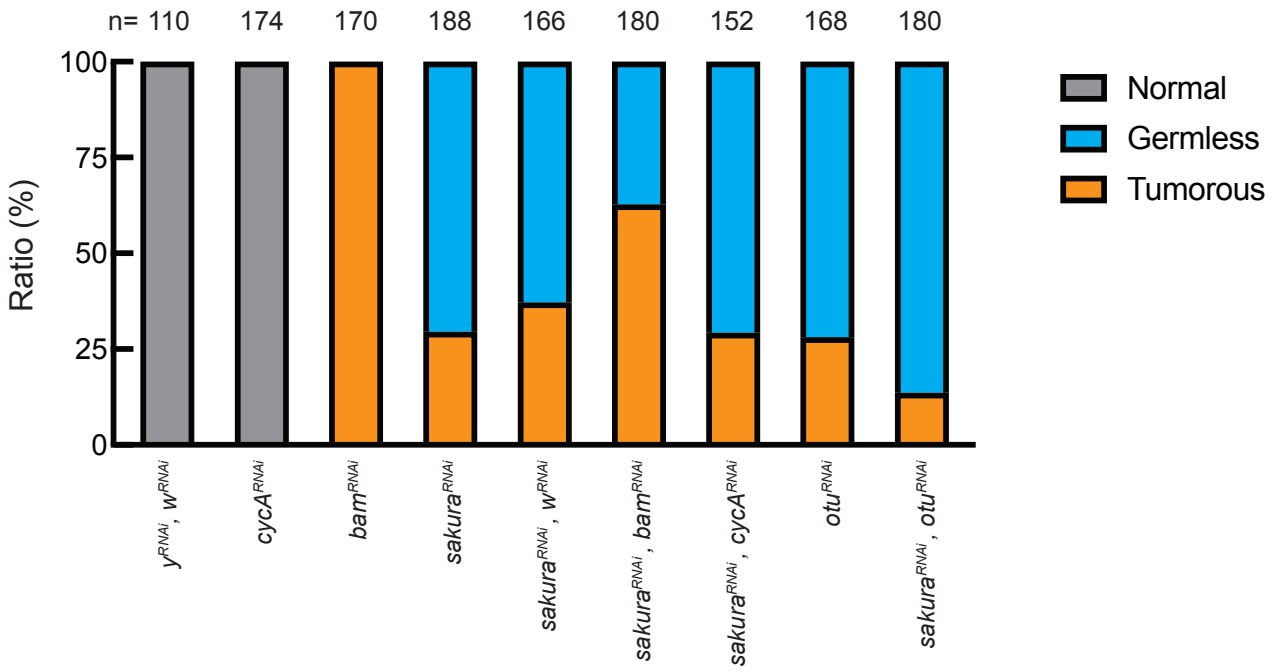

(B)

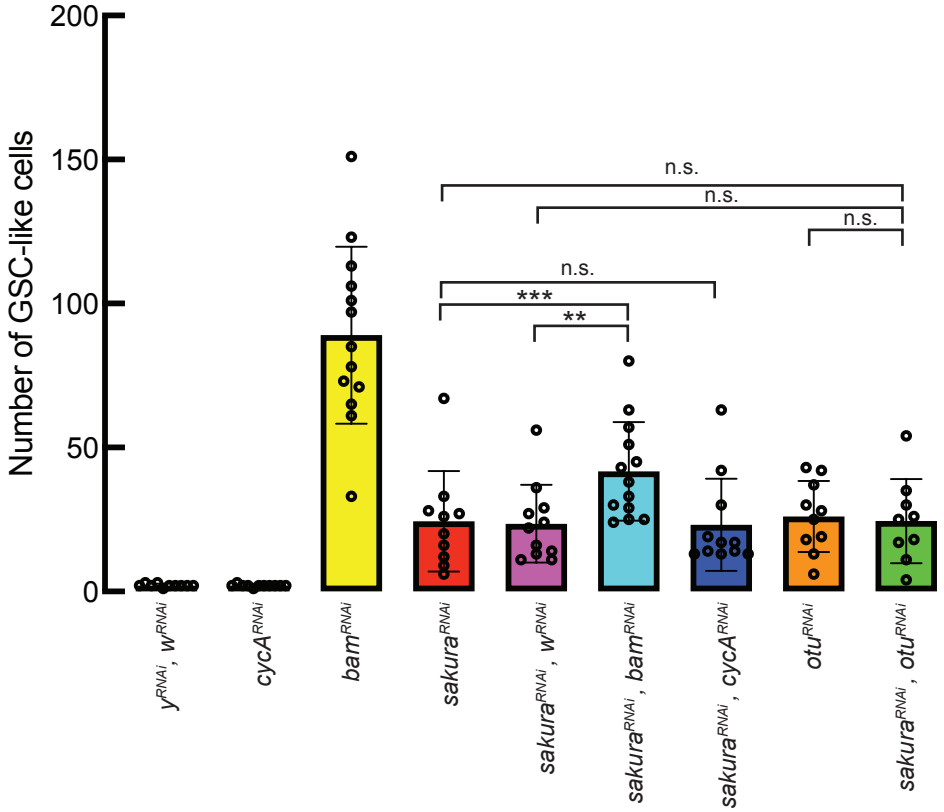

Figure S11. Azlan et al.

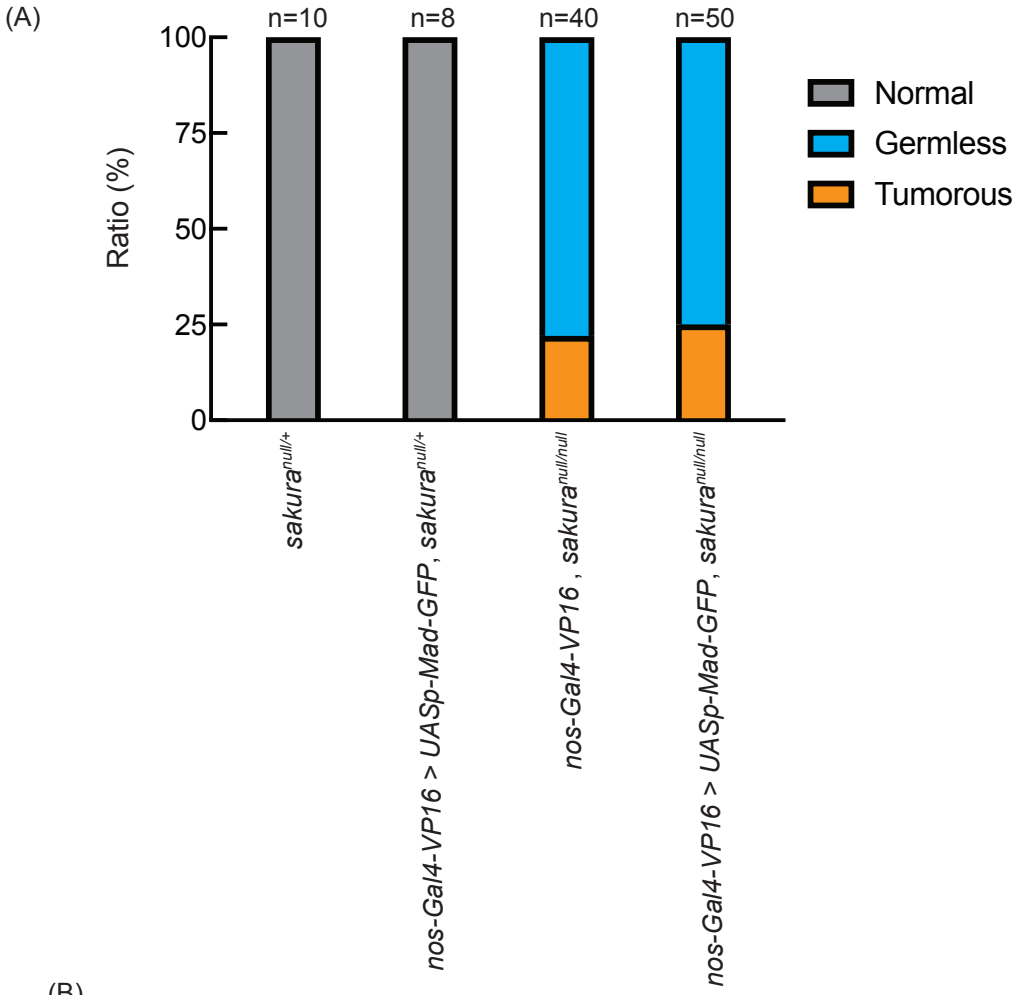

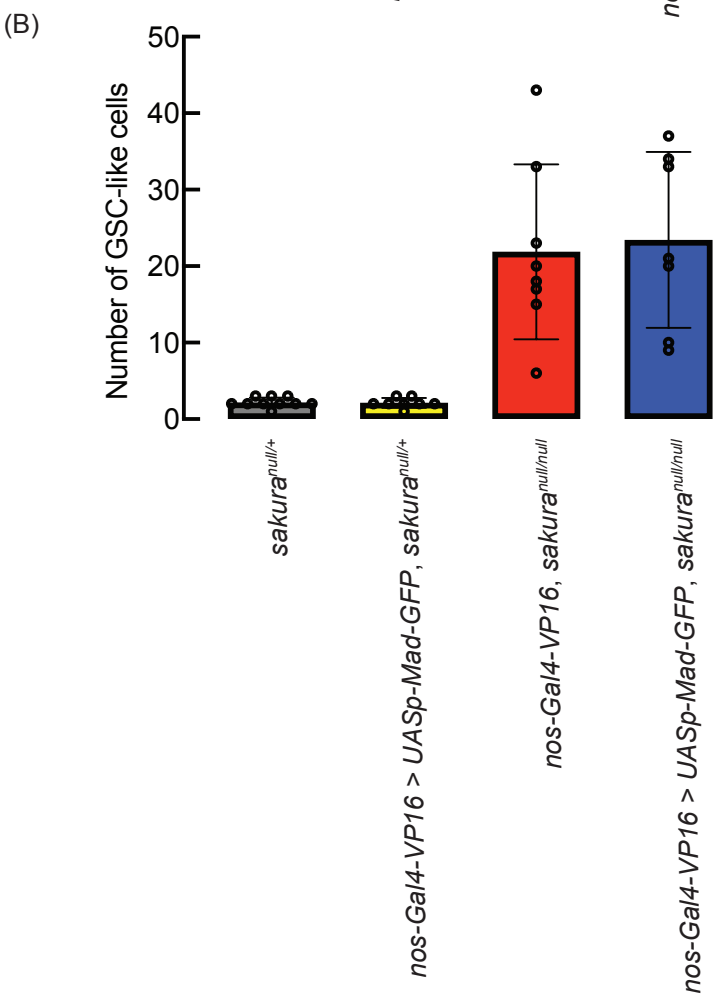

Figure S12. Azlan et al.

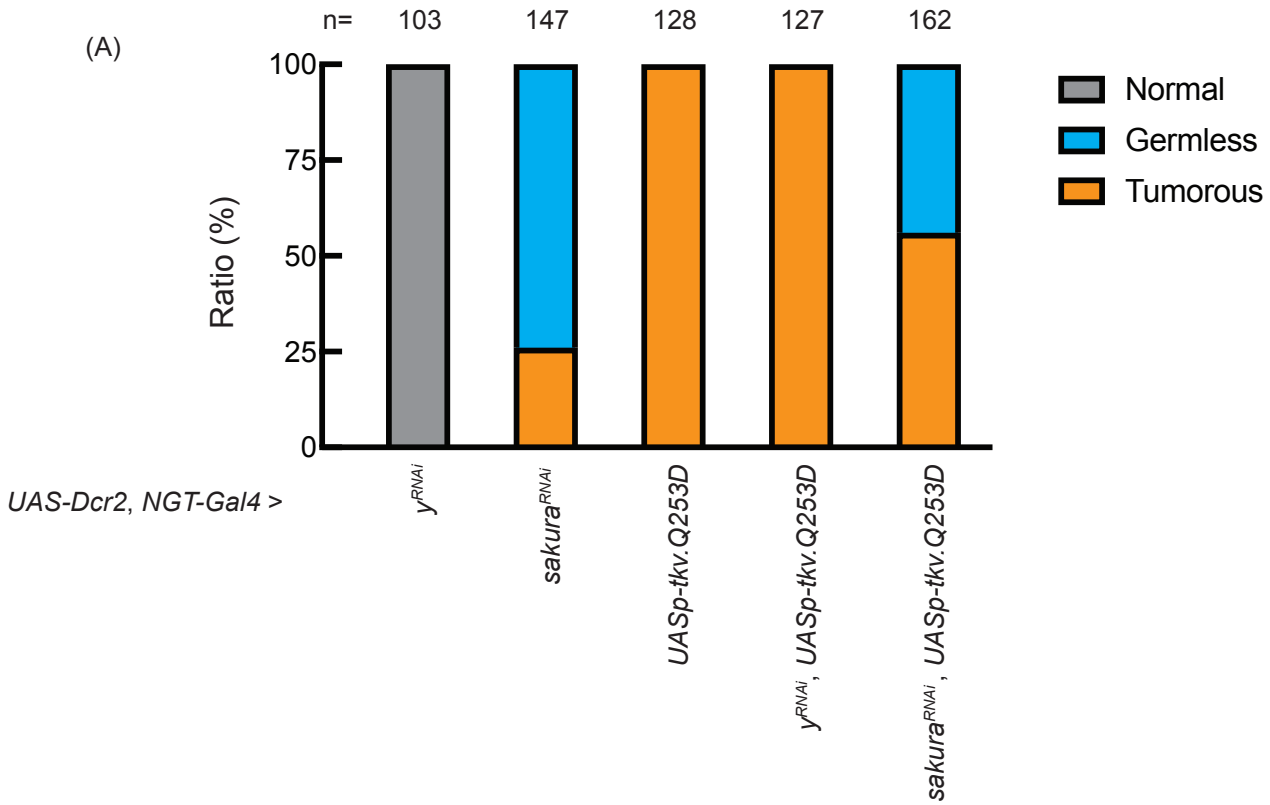

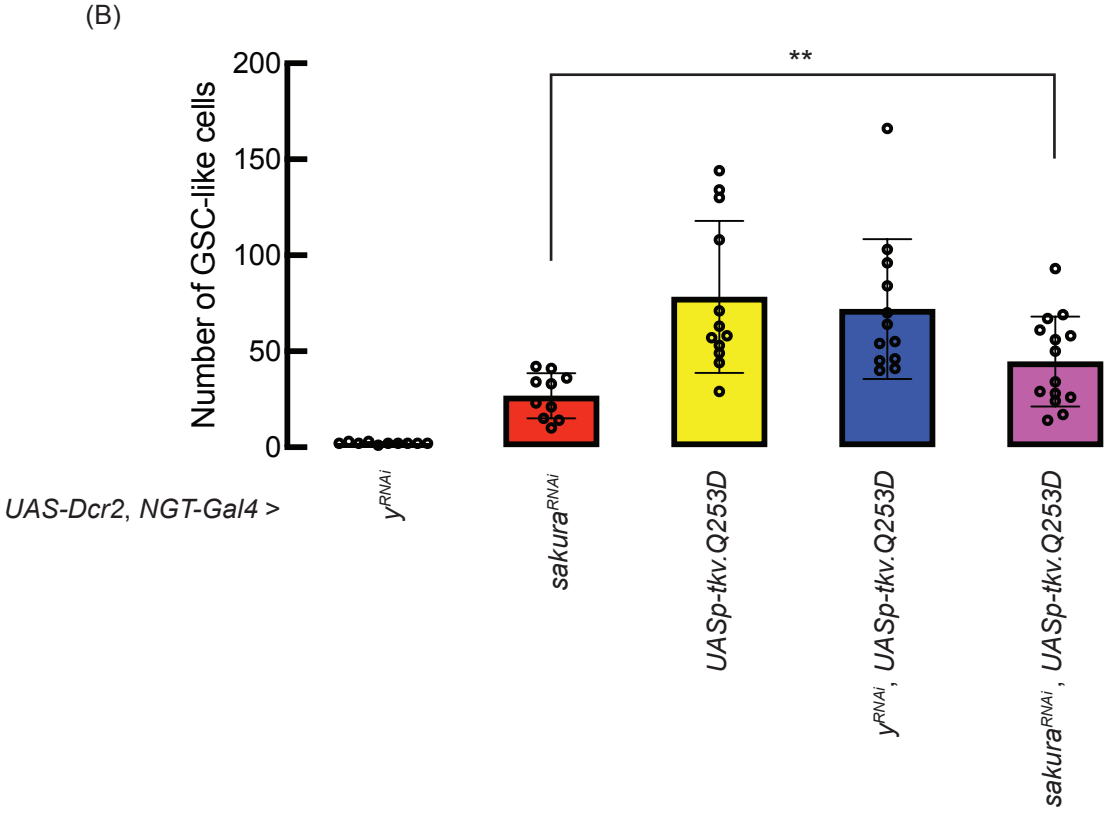

Figure S13. Azlan et al.

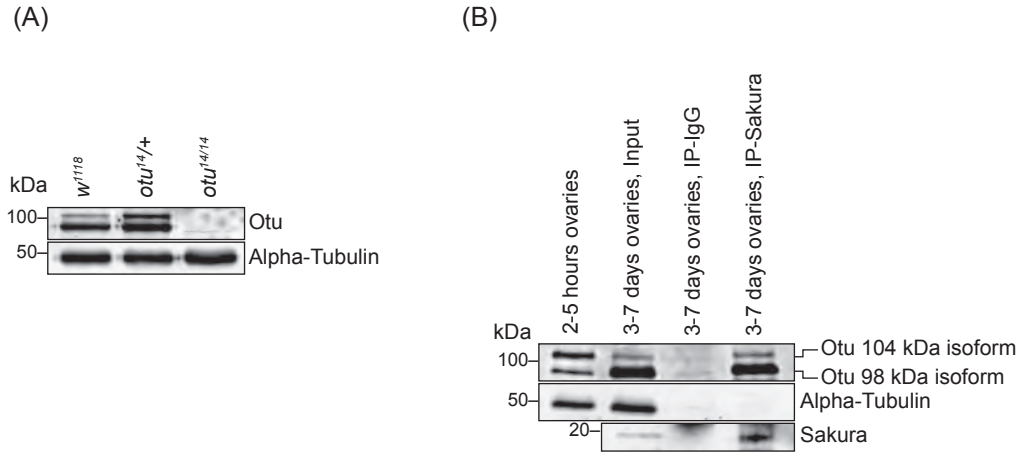

Figure S14. Azlan et al.

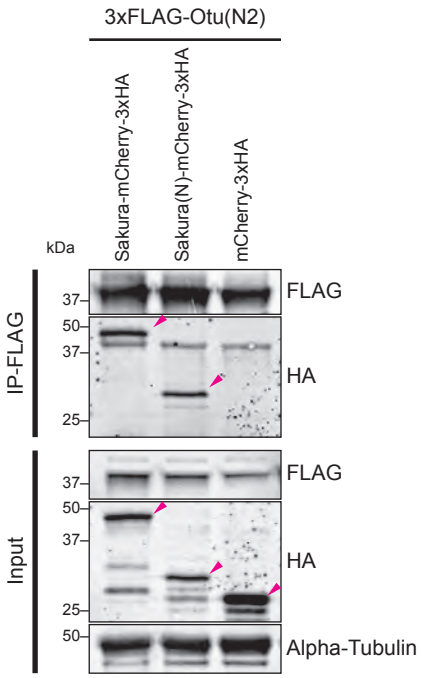

Figure S15. Azlan et al.

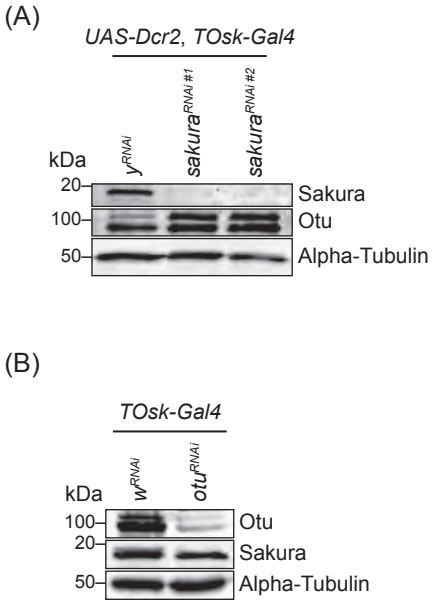
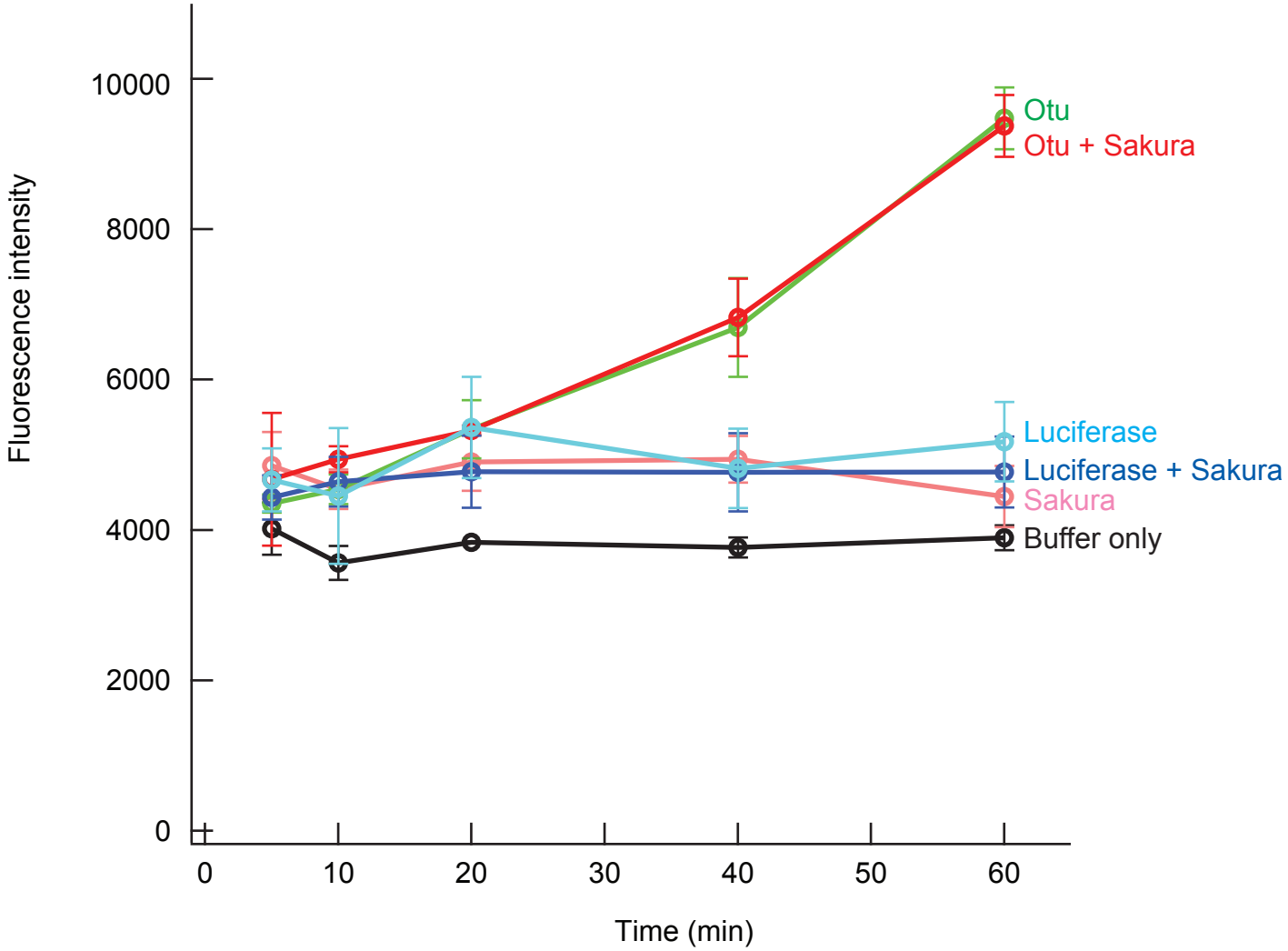
Figure S16. Azlan et al.